

Topological characterization of phase transitions and critical edge states in one-dimensional non-Hermitian systems with sublattice symmetry

Longwen Zhou,^{1,2,3,*} Rujia Jing,¹ and Shenlin Wu¹

¹*College of Physics and Optoelectronic Engineering,
Ocean University of China, Qingdao, China 266100*

²*Key Laboratory of Optics and Optoelectronics, Qingdao, China 266100*

³*Engineering Research Center of Advanced Marine Physical Instruments and Equipment of MOE, Qingdao, China 266100*

(Dated: 2025-09-03)

Critical edge states appear at the bulk gap closing points of topological transitions. Their emergence signify the existence of topologically nontrivial critical points, whose descriptions fall outside the scope of gapped topological matter. In this work, we reveal and characterize topological critical points and critical edge states in non-Hermitian systems. By applying the Cauchy's argument principle to two characteristic functions of a non-Hermitian Hamiltonian, we obtain a pair of winding numbers, whose combination yields a complete description of gapped and gapless topological phases in one-dimensional, two-band non-Hermitian systems with sublattice symmetry. Focusing on a broad class of non-Hermitian Su-Schrieffer-Heeger chains, we demonstrate the applicability of our theory for characterizing gapless symmetry-protected topological phases, topologically distinct critical points, phase transitions along non-Hermitian phase boundaries and their associated topological edge modes. Our findings not only generalize the concepts of topologically nontrivial critical points and critical edge modes to non-Hermitian setups, but also yield additional insights for analyzing topological transitions and bulk-edge correspondence in open systems.

I. INTRODUCTION

Non-Hermitian physics has attracted great attention in the past decades (see [1–17] for reviews). Unique non-Hermitian phenomena, such as the exceptional point [18–23], non-Hermitian skin effect [24–29] and enriched classification of topological matter [31–36] have been discovered theoretically and explored further in experiments, yielding new perspectives on sensing, wave-guiding and other device applications [37–43]. In the study of non-Hermitian topological matter, the focus is mainly rested on systems whose nontrivial topology is associated to a point or a line spectral gap, in which symmetry-protected topological edge states reside [5]. When the bulk spectral gap closes, a phase transition is expected to occur. There, standard topological markers of gapped phases like the winding and Chern numbers become ill-defined. The fates of edge modes related to these topological invariants in nearby gapped phases would also be unclear at the exact transition point. The possibility of finding edge states rooted in the nontrivial topology of non-Hermitian gapless critical points has yet to be unveiled.

Recently, the study of symmetry-protect topological (SPT) phases has been extended to gapless situations [44–84]. The theoretical description of a gapless SPT (gSPT) state not only goes beyond the Landau paradigm of phase transitions based on local order parameters and symmetry-breaking [85], but also falls outside the standard classification of topological insulators and superconductors following the tenfold way [86]. In the simplest case, a gSPT phase can be realized by a critical point between two topologically nontrivial phases [69].

In one spatial dimension, such a realization could be the transition point between two gapped phases with different and nonzero topological invariants in a spin or superconducting chain [47], and the nontrivial topology of the critical point is signified by the presence of degenerate edge modes at the gap-closing point of the bulk energy spectrum [54]. Be coexisting with a gapless bulk, these topological edge modes can also be regarded as critical. In the presence of non-Hermitian effects, the description of gSPT phases could become more complicated. On the one hand, unique non-Hermitian topology related to the exceptional point and non-Bloch band theory may lead to new forms of gSPT phases beyond closed-system constraints. On the other hand, gain and loss or nonreciprocal effects may influence the existence and stability of critical edge modes in an originally Hermitian gSPT phase. Addressing these issues could not only extend the conception of gSPT phases to non-Hermitian setups, but also offer potential insights for further explorations of mixed-state topology [87–92] and bulk-edge correspondence in gapless open systems.

In this work, we propose a theoretical framework to characterize topologically nontrivial critical points and critical edge states in one-dimensional (1D), two-band non-Hermitian systems. Our approach is applicable to the description of both gapped and gapless sublattice-symmetry-protected topological phases. Moreover, it does not concern whether the underlying non-Hermitian band theory is in Bloch (with standard Brillouin zone) or non-Bloch (with generalized Brillouin zone) form. The rest of the paper is organized as follow. In Sec. II, we formulate the definition of topological invariants and the related bulk-edge correspondence in our theory. The topological invariants are deduced from the algebraic zero-pole counting of two characteristic polynomials for a

* zhoulw13@u.nus.edu

given non-Hermitian Hamiltonian. In Sec. III, we apply our theory to characterize the topological phases, phase transitions and edge states in a broad class of non-Hermitian Su-Schrieffer-Heeger (NHSSH) chains, with a focus on the topological nature and bulk-edge correspondence at their gapless critical points. Different classes of topologically distinct critical points and phase transitions along topological phase boundaries are revealed, and the configuration of their critical edge modes are identified. In Sec. IV, we summarize our results and discuss potential future studies. Some calculation details about the non-Hermitian topological edge states are presented in Appendix A.

II. THEORY

In this section, we outline the theoretical framework we proposed to characterize gapped and gapless topological phases in 1D, two-band non-Hermitian systems with sublattice symmetry. Despite showing the basic formulation, we also discuss the issues of some previous theories on the topological characterization of phase transition points with vanishing bulk gaps and critical edge states. The application of our theory to concrete models is presented in the next section.

Under an appropriate basis choice, the generic Hamiltonian of a 1D, two-band, sublattice-symmetric non-Hermitian model can always be expressed in an off-diagonal form as

$$H(k) = \begin{bmatrix} 0 & f(k) \\ g(k) & 0 \end{bmatrix}, \quad (1)$$

where $k \in [-\pi, \pi]$ is the quasimomentum. The off-diagonal elements $f(k)$ and $g(k)$ are both 2π -periodic in k , and the $H(k)$ is non-Hermitian if there exists a quasimomentum k such that $f(k) \neq g^*(k)$. The sublattice symmetry of $H(k)$ is given by $\Gamma = \sigma_z$, in the sense that $\Gamma H(k) \Gamma = -H(k)$ and $\Gamma^2 = \sigma_0$, where σ_0 denotes the 2×2 identity matrix. The Hamiltonian $H(k)$ has two energy bands, whose dispersion relations are given by

$$E_{\pm}(k) \equiv \pm E(k) = \pm \sqrt{f(k)g(k)}. \quad (2)$$

The right eigenvectors of $H(k)$ has the form $\psi(k) \sim [a(k), b(k)]^T$, where the components $a(k)$ and $b(k)$ satisfy

$$\frac{b(k)}{a(k)} = \frac{E(k)}{f(k)} = \frac{g(k)}{E(k)}. \quad (3)$$

Therefore, all the information about the eigensystem of $H(k)$ are contained in the ratio $[b(k)/a(k)]^2 = g(k)/f(k)$ and the product $E^2(k) = f(k)g(k)$. We refer to these two functions as the characteristic functions of $H(k)$, and

express them as

$$P(k) \equiv \frac{g(k)}{f(k)}, \quad Q(k) \equiv f(k)g(k). \quad (4)$$

These functions are also expected to encode the topological properties and phase transitions of the system described by $H(k)$.

As the $f(k)$ and $g(k)$ are 2π -periodic in k , the characteristic functions $P(k)$ and $Q(k)$ should also satisfy $P(k + 2\pi) = P(k)$ and $Q(k + 2\pi) = Q(k)$. We could thus expand the $P(k)$ and $Q(k)$ into Fourier series as $P(k) = \sum_{n \in \mathbb{Z}} p_n e^{in k}$ and $Q(k) = \sum_{n \in \mathbb{Z}} q_n e^{in k}$. These series can be viewed as polynomials of the exponential factor e^{ik} . To treat Bloch and non-Bloch band theories of non-Hermitian systems on an equal footing, we extend the e^{ik} to the whole complex plane by setting $e^{ik} \rightarrow z$ with $z \in \mathbb{C}$. The resulting characteristic polynomials of the complex-extended Hamiltonian $H(z)$ are given by $P(z) = \sum_{n \in \mathbb{Z}} p_n z^n$ and $Q(z) = \sum_{n \in \mathbb{Z}} q_n z^n$, or

$$P(z) = \frac{g(z)}{f(z)}, \quad Q(z) = f(z)g(z), \quad (5)$$

where $f(z) \equiv f(k \rightarrow -i \ln z)$ and $g(z) \equiv g(k \rightarrow -i \ln z)$ are ‘‘complex continuations’’ of $f(k)$ and $g(k)$. Inside a closed contour on the complex z -plane, the difference between the numbers of zeros and poles (including their multiplicities and orders) of $P(z)$ and $Q(z)$ yield two integer-quantized winding numbers W_1 and W_2 , respectively, according to the Cauchy’s argument principle. Our theoretical proposal is based on the topological messages encoded in these winding numbers.

In previous studies [27, 30], it was found that by identifying the first $2\mu = 2 \max\{m, n\}$ zeros and/or poles of $P(z)$ (ordered according to their magnitudes), we would obtain a winding number $W_0 \equiv N_z^{\in 2\mu} - N_p^{\in 2\mu}$, which could characterize each topological phase of a 1D, two-band, sublattice-symmetric non-Hermitian system and determine the number N_0 of its edge zero modes via the relation $N_0 = |W_0|$. Here, m and n are given by the highest negative powers of $f(z)$ and $g(z)$ in z . $N_z^{\in 2\mu}$ and $N_p^{\in 2\mu}$ are the numbers of zeros and poles of $P(z)$ inside the set of its first 2μ zeros/poles. This algebraic approach is proved to be equivalent to other methods based on the generalized Brillouin zone (GBZ) and non-Bloch band theory for gapped phases [25, 26, 30]. However, this $P(z)$ -based theory may lead to ambiguous predictions about the non-Hermitian topology and edge states at phase transition points, where the Bloch or non-Bloch bands of the system are touched at zero energy.

The above point can be made clear via a counterexample. Let us consider a complex-continued non-Hermitian Hamiltonian $H(z)$ with off-diagonal elements $f(z) = J_0 + J_1 z^{-1}$ and $g(z) = J_0 + J_1 z$. When J_0 and J_1 take real values, we go back to the standard SSH model after setting $z \rightarrow e^{ik}$. Following the $P(z)$ -based approach, we have $m = 1$, $n = 0$ and thus $2\mu = 2 \max\{1, 0\} = 2$. By defini-

tion, we find $P(z) = g(z)/f(z) = z(J_0 + J_1 z)/(J_0 z + J_1)$. It can then be identified that if $|J_1| < |J_0|$, the first 2 zeros/poles of $P(z)$ contains a zero at $z = 0$ and a pole at $z = -J_1/J_0$, yielding $N_z^{\epsilon^2} = 1$, $N_p^{\epsilon^2} = 1$, $W_0 = N_z^{\epsilon^2\mu} - N_p^{\epsilon^2\mu} = 0$ and $N_0 = |W_0| = 0$. Meanwhile, if $|J_1| > |J_0|$, the first 2 zeros/poles of $P(z)$ contains two zeros at $z = 0$ and $z = -J_0/J_1$, yielding $N_z^{\epsilon^2} = 2$, $N_p^{\epsilon^2} = 0$, $W_0 = N_z^{\epsilon^2\mu} - N_p^{\epsilon^2\mu} = 2$ and $N_0 = |W_0| = 2$. These predictions are all correct, as the two bulk bands of $H(z)$ are gapped at zero energy [$Q(z) \neq 0$] for any finite z whenever $|J_1| \neq |J_0|$. However, at the phase transition point $|J_1| = |J_0|$, we have $|-J_1/J_0| = |-J_0/J_1| = 1$, which means that we could not order the magnitudes of the zero and pole at $z = -J_0/J_1$ and $z = -J_1/J_0$. The determination of which are the first two zeros and/or poles of $P(z)$ then becomes ambiguous. If we include or exclude both their contributions to W_0 , we will get $W_0 = 1$ and thus $N_0 = 1$. This is impossible, as the zero modes must come in pairs (i.e., $N_0 \in 2\mathbb{N}$) due to the sublattice symmetry. If we only retain the zero at $z = -J_0/J_1$ as the second zero/pole, we will get $W_0 = 2$ and $N_0 = 2$, which is incorrect even for the Hermitian SSH model [46]. If we instead retain the pole at $z = -J_1/J_0$ as the second zero/pole, we will find $W_0 = 0$ and $N_0 = 0$. Even though these are the correct values of topological invariants and edge states at the critical point of standard SSH model [46], they could not be conclusively and unambiguously predicted by the $P(z)$ -based approach. Therefore, the algebraic scheme in Refs. [27, 30] tends out to be inapplicable to the characterization of nontrivial topology and bulk-edge correspondence at the phase transition (bulk-gap closing) point of non-Hermitian systems. Similarly, as the algebraic and GBZ schemes are proved to be equivalent for sublattice-symmetric models [30], the standard GBZ approach is also expected to be unworkable for describing gSPT phases in non-Hermitian systems.

These observations motivate us to generalize existing theories in order to characterize the nontrivial topology at non-Hermitian critical points. The above example suggests that there could be competing zeros and poles of equal magnitudes in $P(z)$, whose topological signatures may subject to cancellations at the critical point. Their contributions are instead all retained in the characteristic function $Q(z)$ as its zeros at the gap closing point. Therefore, we propose to introduce an additional winding number by applying the Cauchy's argument principle to $Q(z)$. More precisely, we take the GBZ as the integration contour of the argument principle. The winding numbers of $P(z)$ and $Q(z)$ are then given by

$$\begin{aligned} W_1 &\equiv N_{1z}^{\in \text{GBZ}} - N_{1p}^{\in \text{GBZ}}, \\ W_2 &\equiv N_{2z}^{\in \text{GBZ}} - N_{2p}^{\in \text{GBZ}}. \end{aligned} \quad (6)$$

Here, $N_{1z}^{\in \text{GBZ}}$ and $N_{1p}^{\in \text{GBZ}}$ ($N_{2z}^{\in \text{GBZ}}$ and $N_{2p}^{\in \text{GBZ}}$) denote the numbers of zeros and poles of $P(z)$ ($Q(z)$) inside the GBZ. Note that the definition of W_1 is consistent with

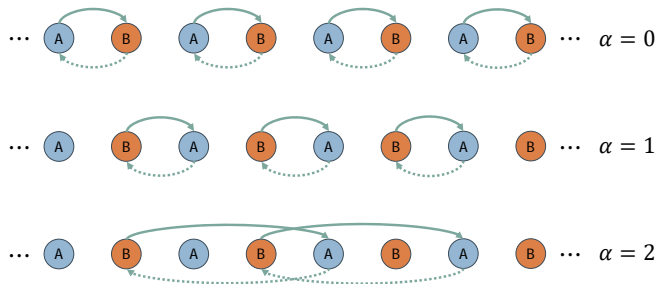


FIG. 1. Schematic illustration of NHSSH α chains with $\alpha = 0, 1, 2$. In each case, the solid and dotted curves with arrows denote hopping amplitudes from left to right and right to left between sublattices A (cyan balls) and B (orange balls).

the definition of W_0 in the existing theory [30]. Combining the information encoded in W_1 and W_2 , we arrive at the final topological invariant W and bulk-edge correspondence of 1D, two-band systems with sublattice symmetry, i.e.,

$$W = \frac{W_1 + W_2}{2}, \quad (7)$$

$$N_0 = |W_1 + W_2| = 2|W|, \quad (8)$$

where N_0 denotes the total number of edge zero modes.

One may now check the applicability of our theory to the simplest SSH model. Besides the $P(z) = z(J_0 + J_1 z)/(J_0 z + J_1)$, we also have $Q(z) = (J_0 z + J_1)(J_0 + J_1 z)/z$. The GBZ here is just the standard Brillouin zone, which forms a circle of radius 1 on the complex plane regardless of whether the values of J_0 and J_1 are real or complex. Direct calculations following Eqs. (6)–(8) predict $(W_1, W_2) = (0, 0)$ when $|J_1| < |J_0|$, $(W_1, W_2) = (2, 0)$ when $|J_1| > |J_0|$, and $(W_1, W_2) = (1, -1)$ when $|J_1| = |J_0|$, yielding $W = 0, 1, 0$ and $N_0 = 0, 2, 0$ in these three parameter regions. Besides reproducing known results about gapped phases [93], we also confirm the topological triviality of the gapless phase boundary $|J_1| = |J_0|$ of the SSH model [47] without ambiguity. In the next section, we utilize our theory to depict the topology and edge states in both gapped phases and along gapless phase boundaries for a broad class of sublattice-symmetric non-Hermitian models.

III. RESULTS

In this section, we demonstrate the applicability of our theory to the characterization of topologically nontrivial critical points and zero-energy edge modes in non-Hermitian systems. We first introduce a general class of 1D non-Hermitian models with sublattice symmetry in Sec. III A, which will be referred to as NHSSH α chains. Our theory is then applied to describing gapped topological phases, distinguishing between topologically trivial and nontrivial critical points, and depicting topolog-

ical phase transitions without gap closing/reopening in Secs. III B, III C, and III D, respectively, for three different types of NHSSH α chains. Theoretical analyses are complemented by numerical calculations of the spectra and edge states in each case.

A. Model

The generic NHSSH α chain is formally described by the Hamiltonian $\hat{H} = \sum_{\alpha \in \mathbb{Z}} \hat{H}_\alpha$, where

$$\hat{H}_\alpha = \sum_{n \in \mathbb{Z}} \left(J_\alpha^L \hat{b}_n^\dagger \hat{a}_{n+\alpha} + J_\alpha^R \hat{a}_{n+\alpha}^\dagger \hat{b}_n \right), \quad J_\alpha^L, J_\alpha^R \in \mathbb{C}. \quad (9)$$

The \hat{a}_n^\dagger (\hat{b}_n^\dagger) creates a particle in the sublattice A (B) of unit cell n . J_α^L (J_α^R) denotes the hopping amplitude from right to left (left to right) over α lattice sites. The \hat{H} is non-Hermitian whenever there exists an α such that $J_\alpha^L \neq (J_\alpha^R)^*$. The Hermitian SSH model is recovered by setting $\hat{H} = \sum_{\alpha=0,1} \hat{H}_\alpha$ and $J_\alpha^L = J_\alpha^R = J_\alpha \in \mathbb{R}$. The lattice geometries of \hat{H}_α with $\alpha = 0, 1, 2$ are shown in Fig. 1.

Under the periodic boundary condition (PBC), we can express the Hamiltonian \hat{H} in momentum space via Fourier transformations

$$\hat{a}_n = \frac{1}{\sqrt{N}} \sum_k e^{ikn} \hat{a}_k, \quad \hat{b}_n = \frac{1}{\sqrt{N}} \sum_k e^{ikn} \hat{b}_k, \quad (10)$$

where N is the total number of unit cells and $k \in [-\pi, \pi]$ denotes the quasimomentum. In momentum space, the component \hat{H}_α has the form $\hat{H}_\alpha = \sum_k \hat{\Psi}_k^\dagger H_\alpha(k) \hat{\Psi}_k$, where $\hat{\Psi}_k^\dagger \equiv (\hat{a}_k^\dagger, \hat{b}_k^\dagger)$. The $H_\alpha(k)$ is a 2×2 off-diagonal matrix of the form

$$H_\alpha(k) = \begin{bmatrix} 0 & J_\alpha^R e^{-ik\alpha} \\ J_\alpha^L e^{ik\alpha} & 0 \end{bmatrix}. \quad (11)$$

It is clear that each $H_\alpha(k)$ [and also the combined Bloch Hamiltonian $H(k) = \sum_{\alpha \in \mathbb{Z}} H_\alpha(k)$] has the sublattice symmetry $\Gamma = \sigma_z$, in the sense that $\Gamma H_\alpha(k) \Gamma = -H_\alpha(k)$ and $\Gamma^2 = \sigma_0$ for any α . The theoretical framework developed in the last section is thus applicable. Making the substitution $e^{ik} \rightarrow z$ with $z \in \mathbb{C}$, we find the extension of $H_\alpha(k)$ to the whole complex plane as

$$H_\alpha(z) = \begin{bmatrix} 0 & J_\alpha^R z^{-\alpha} \\ J_\alpha^L z^\alpha & 0 \end{bmatrix}. \quad (12)$$

The extended Bloch Hamiltonian of the NHSSH α chain is then given by $H(z) = \sum_{\alpha \in \mathbb{Z}} H_\alpha(z)$.

In the following, we consider three different types of NHSSH α chains. We apply our theory to characterize the topological phases and bulk-edge correspondence of the system in each case.

B. Single α chain: gapped and gapless phases

The NHSSH single α chain has the complex-extended Hamiltonian $H(z) = H_\alpha(z)$. It contains only a single length scale in its hopping amplitudes $J_\alpha^{L,R}$. In this subsection, we assume $\alpha \geq 0$ without losing generality.

Following the theoretical development in Sec. II, we find $f(z) = J_\alpha^R z^{-\alpha}$ and $g(z) = J_\alpha^L z^\alpha$ for the single α chain. The characteristic functions are thus given by

$$P(z) = \frac{J_\alpha^L}{J_\alpha^R} z^{2\alpha}, \quad Q(z) = J_\alpha^L J_\alpha^R. \quad (13)$$

Since the $Q(z) = [E(z)]^2$ is independent of z , the bulk spectrum of the system is formed by two flat bands at $\pm E(z) = \pm \sqrt{J_\alpha^L J_\alpha^R}$, and the GBZ is just the standard BZ with $k \in [-\pi, \pi]$. On the complex z -plane, the $Q(z)$ has neither zeros nor poles, while the $P(z)$ has a zero of order 2α at $z = 0$, which is inside the BZ unit circle $|z| = 1$. According to the definition of winding numbers for $P(z)$ and $Q(z)$ in Eq. (6), we find $W_1 = 2\alpha$ and $W_2 = 0$. The topological invariant W of the system and the number of its degenerate zero modes N_0 under the open boundary condition (OBC) are thus given by Eqs. (7) and (8) as

$$W = \frac{W_1 + W_2}{2} = \alpha, \quad N_0 = 2|W| = 2\alpha. \quad (14)$$

We find that the topological phase of the system is independent of its hopping amplitudes, so long as the J_α^L and J_α^R are not simultaneously zero. Meanwhile, the bulk spectrum of the system is gapped (gapless) when $J_\alpha^L \neq 0$ and $J_\alpha^R \neq 0$ ($J_\alpha^L = 0$ or $J_\alpha^R = 0$). The NHSSH single α chain could thus admit both gapped and gapless topologically nontrivial phases whenever $\alpha \neq 0$.

We now verify our results about the NHSSH single α chain with two groups of numerical examples. In the first group, we consider the case of asymmetric hopping with $(J_\alpha^L, J_\alpha^R) = (0.5, 2)$ for $\alpha = 0, 1, 2$. The bulk spectrum is expected to show two flat bands at $\pm \sqrt{J_\alpha^L J_\alpha^R} = \pm 1$, separated by a constant gap $\Delta E = 2$. In the second group, we consider the case of unidirectional hopping with $(J_\alpha^L, J_\alpha^R) = (0, 1)$ for $\alpha = 0, 1, 2$. The bulk spectrum is expected to show two degenerate flat bands at zero energy. In these three cases, the theoretically predicted winding numbers and numbers of zero-energy edge modes are $W = (0, 1, 2)$ and $N_0 = (0, 2, 4)$ according to Eq. (14), regardless of the chosen parameter values (J_α^L, J_α^R) .

In Fig. 2, we present the energy spectra and edge states of the single α chain for $\alpha = 0, 1, 2$ and $(J_\alpha^L, J_\alpha^R) = (0.5, 2)$. The spectrum of \hat{H}_0 in Fig. 2(a) has no signatures of zero-energy edge modes ($N_0 = 0$). The spectrum of \hat{H}_1 in Fig. 2(b) possesses two zero-energy edge modes ($N_0 = 2$), whose probability distributions are shown in Fig. 2(d). The spectrum of \hat{H}_2 in Fig. 2(c) has four zero-energy edge modes ($N_0 = 4$), whose probability distributions are shown in Fig. 2(e). These numerical results are all consistent with our theoretical predictions.

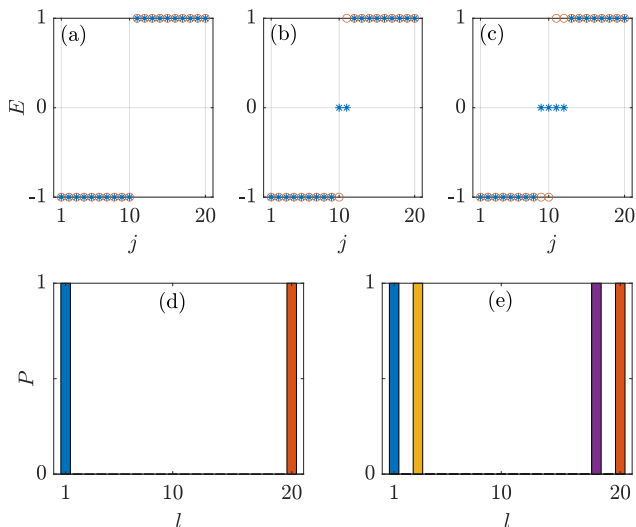


FIG. 2. Spectra and edge states of NHSSH single α chains with bulk gaps. The system has 10 unit cells and 20 lattice sites. j is the state index. l is the lattice index. (a) Energy spectrum of \hat{H}_0 with $(J_0^L, J_0^R) = (0.5, 2)$ under the PBC (in circles) and OBC (in stars). (b) Energy spectrum of \hat{H}_1 with $(J_1^L, J_1^R) = (0.5, 2)$ under the PBC (in circles) and OBC (in stars). (c) Energy spectrum of \hat{H}_2 with $(J_2^L, J_2^R) = (0.5, 2)$ under the PBC (in circles) and OBC (in stars). (d) Probability distributions P of the zero-energy edge states of \hat{H}_1 in (b). (e) Probability distributions P of the zero-energy edge states of \hat{H}_2 in (c). In (d) and (e), different edge states are distinguished by the colors of probability bars.

In Fig. 3, we present the energy spectra and edge states of the single α chain for $\alpha = 0, 1, 2$ and $(J_\alpha^L, J_\alpha^R) = (0, 1)$. The spectrum of \hat{H}_0 in Fig. 3(a) has no edge zero modes ($N_0 = 0$). The spectrum of \hat{H}_1 in Fig. 3(b) holds two zero-energy edge modes ($N_0 = 2$), whose distributions are shown in Fig. 3(d). The spectrum of \hat{H}_2 in Fig. 3(c) contains four zero-energy edge modes ($N_0 = 4$), whose distributions are shown in Fig. 3(e). These results again verify our theoretical predictions. Notably, even though the bulk spectra of $\hat{H}_{0,1,2}$ have no gaps at $E = 0$ in Figs. 3(a)–3(c), our theory could still correctly predict the numbers of edge zero modes that can coexist with gapless bulks in these cases.

The presence or absence of edge zero modes in the spectrum of \hat{H}_α for a given α can be understood from the geometric connectivity of the underlying lattice (see Fig. 1). For \hat{H}_0 , the sublattices A and B in each unit cell are coupled due to the non-vanishing J_0^L and/or J_0^R , making it impossible to have isolated sites at boundaries to host edge zero modes. For \hat{H}_1 , the sublattice B in unit cell n is coupled to the sublattice A in unit cell $n + 1$ for $n = 1, \dots, N - 1$. The sublattices A in unit cell 1 and B in unit cell N are thus isolated from other sites, making them available to host two edge zero modes $\hat{a}_1^\dagger|\emptyset\rangle$ and $\hat{b}_N^\dagger|\emptyset\rangle$, where $|\emptyset\rangle$ denotes the vacuum state. For \hat{H}_2 , the sublattice B in unit cell n is coupled to the sublattice A

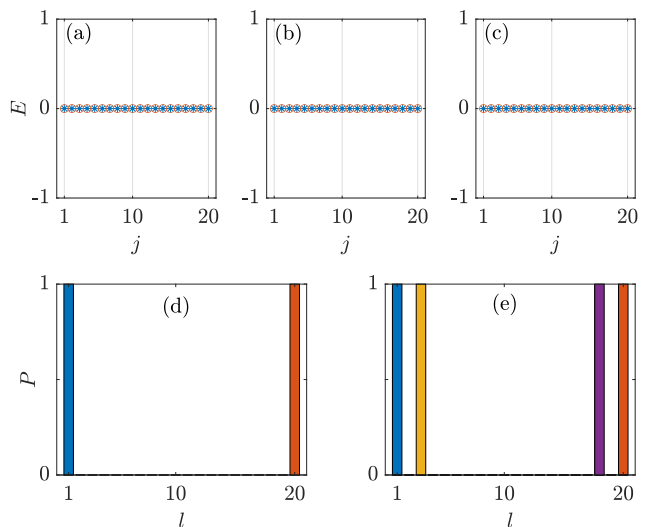


FIG. 3. Spectra and edge states of NHSSH single α chains without bulk gaps. The system has 10 unit cells and 20 lattice sites. j is the state index. l is the lattice index. (a) Energy spectrum of \hat{H}_0 with $(J_0^L, J_0^R) = (0, 1)$ under the PBC (in circles) and OBC (in stars). (b) Energy spectrum of \hat{H}_1 with $(J_1^L, J_1^R) = (0, 1)$ under the PBC (in circles) and OBC (in stars). (c) Energy spectrum of \hat{H}_2 with $(J_2^L, J_2^R) = (0, 1)$ under the PBC (in circles) and OBC (in stars). (d) Probability distributions P of the zero-energy edge states of \hat{H}_1 in (b). (e) Probability distributions P of the zero-energy edge states of \hat{H}_2 in (c). In (d) and (e), different edge states are distinguished by the colors of probability bars.

in unit cell $n + 2$ for $n = 1, \dots, N - 2$. The sublattices A in unit cells 1, 2 and B in unit cells $N - 1, N$ are thus isolated from other sites, making them available to host four edge zero modes $\hat{a}_1^\dagger|\emptyset\rangle, \hat{a}_2^\dagger|\emptyset\rangle, \hat{b}_{N-1}^\dagger|\emptyset\rangle$ and $\hat{b}_N^\dagger|\emptyset\rangle$. It is also clear that the topological origin of zero-energy edge modes in a single α chain does not depend on whether the system is Hermitian or non-Hermitian.

In the next two subsections, we study NHSSH α chains with topologically distinct critical points and critical edge zero modes.

C. (α, α') chain: topologically trivial/nontrivial critical points

The NHSSH (α, α') chain has the complex-extended Hamiltonian $H(z) = H_\alpha(z) + H_{\alpha'}(z)$, where $\alpha \neq \alpha'$. It has two competing length scales in its hopping amplitudes $J_\alpha^{L,R}$ and $J_{\alpha'}^{L,R}$, making it possible to find topological phase transitions. We assume $0 \leq \alpha < \alpha'$ throughout this subsection. The cases with $\alpha, \alpha' \leq 0$ can be treated following a similar routine.

The theoretical development in Sec. II allows us to identify $f(z) = J_\alpha^R z^{-\alpha} + J_{\alpha'}^R z^{-\alpha'}$ and $g(z) = J_\alpha^L z^\alpha + J_{\alpha'}^L z^{\alpha'}$ for the (α, α') chain. The characteristic functions

$P(z)$ and $Q(z)$ are thus given by

$$P(z) = \frac{J_\alpha^L z^\alpha + J_{\alpha'}^L z^{\alpha'}}{J_\alpha^R z^{-\alpha} + J_{\alpha'}^R z^{-\alpha'}}, \quad (15)$$

$$Q(z) = (J_\alpha^L z^\alpha + J_{\alpha'}^L z^{\alpha'})(J_\alpha^R z^{-\alpha} + J_{\alpha'}^R z^{-\alpha'}). \quad (16)$$

It is straightforward to inspect that $P(z)$ has a zero of order $(\alpha' + \alpha)$ at $z = 0$, other $(\alpha' - \alpha)$ zeros of order 1 along the circle of radius $r^L = |J_\alpha^L/J_{\alpha'}^L|^{1/(\alpha' - \alpha)}$, and $(\alpha' - \alpha)$ poles of order 1 along the circle of radius $r^R = |J_{\alpha'}^R/J_\alpha^R|^{1/(\alpha' - \alpha)}$. On the other hand, $Q(z)$ has $(\alpha' - \alpha)$ zeros of order 1 along the circle of radius r^L , other $(\alpha' - \alpha)$ zeros of order 1 along the circle of radius r^R , and a pole of order $(\alpha' - \alpha)$ at $z = 0$. The locations of these zeros and poles relative to the GBZ fully determine the topology of gapped phases and gapless phase boundaries of the (α, α') chain.

The GBZ of NHSSH (α, α') chain can be obtained from the two middle solutions of the equation $Q(z) = Q(ze^{i\theta})$ for $\theta \in [0, 2\pi]$ [26]. Direct calculations yield the solution $z^{2(\alpha' - \alpha)} = J_\alpha^L J_{\alpha'}^R e^{-i(\alpha' - \alpha)\theta} / (J_{\alpha'}^L J_\alpha^R)$. Therefore, the GBZ of the (α, α') chain has the shape of a circle with the radius

$$r_0 = \left| \frac{J_\alpha^L J_{\alpha'}^R}{J_{\alpha'}^L J_\alpha^R} \right|^{\frac{1}{2(\alpha' - \alpha)}}. \quad (17)$$

Under the non-Hermitian condition $J_\alpha^L \neq (J_\alpha^R)^*$ and/or $J_{\alpha'}^L \neq (J_{\alpha'}^R)^*$, we will generally have $r_0 \neq 1$, making the GBZ different from the standard BZ of a Hermitian model that corresponds to a unit circle on the complex plane. The critical (gap-closing) points of the NHSSH (α, α') chain can be obtained by inserting the GBZ solution $z_0 = r_0 e^{i\phi}$ ($\phi \in [0, 2\pi]$) into the equality $Q(z) = [E(z)]^2 = 0$, yielding the phase boundary equation in the hopping parameter space as

$$|J_\alpha^L J_{\alpha'}^R| = |J_{\alpha'}^L J_\alpha^R|. \quad (18)$$

The parameter regions with $|J_\alpha^L J_{\alpha'}^R| < |J_{\alpha'}^L J_\alpha^R|$ and $|J_\alpha^L J_{\alpha'}^R| > |J_{\alpha'}^L J_\alpha^R|$ are then expected to belong to distinct topological phases.

We next determine the locations of zeros/poles of $P(z)$ and $Q(z)$ relative to the GBZ. Using the relevant radius $r^L = |J_\alpha^L/J_{\alpha'}^L|^{1/(\alpha' - \alpha)}$ and $r^R = |J_{\alpha'}^R/J_\alpha^R|^{1/(\alpha' - \alpha)}$, we obtain

$$\frac{r^L}{r_0} = \left| \frac{J_\alpha^L J_{\alpha'}^R}{J_{\alpha'}^L J_\alpha^R} \right|^{\frac{1}{2(\alpha' - \alpha)}}, \quad \frac{r^R}{r_0} = \left| \frac{J_\alpha^L J_{\alpha'}^R}{J_{\alpha'}^L J_\alpha^R} \right|^{\frac{1}{2(\alpha' - \alpha)}}. \quad (19)$$

Therefore, if $|J_\alpha^L J_{\alpha'}^R| < |J_{\alpha'}^L J_\alpha^R|$, the zeros/poles lying along the circles of radius r^L and r^R are outside and inside the GBZ, respectively. On the contrary, when $|J_\alpha^L J_{\alpha'}^R| > |J_{\alpha'}^L J_\alpha^R|$, the zeros/poles lying along the circles of radius r^L and r^R are inside and outside the GBZ, respectively. If $|J_\alpha^L J_{\alpha'}^R| = |J_{\alpha'}^L J_\alpha^R|$, we have $r^L = r^R = r_0$, which means that the zeros/poles along the circles of ra-

dius r^L and r^R are both on the GBZ when the phase boundary is reached. Finally, the zeros and poles at $z = 0$ are all inside the GBZ so long as the GBZ radius $r_0 > 0$.

We could now obtain the winding numbers W_1 and W_2 of $P(z)$ and $Q(z)$ following the Cauchy's argument principle. Specially, we find from the Eq. (6) that

$$W_1 = \begin{cases} 2\alpha, & |J_\alpha^L J_{\alpha'}^R| < |J_{\alpha'}^L J_\alpha^R| \\ \alpha + \alpha', & |J_\alpha^L J_{\alpha'}^R| = |J_{\alpha'}^L J_\alpha^R| \\ 2\alpha', & |J_\alpha^L J_{\alpha'}^R| > |J_{\alpha'}^L J_\alpha^R| \end{cases}, \quad (20)$$

$$W_2 = \begin{cases} 0, & |J_\alpha^L J_{\alpha'}^R| < |J_{\alpha'}^L J_\alpha^R| \\ \alpha - \alpha', & |J_\alpha^L J_{\alpha'}^R| = |J_{\alpha'}^L J_\alpha^R| \\ 0, & |J_\alpha^L J_{\alpha'}^R| > |J_{\alpha'}^L J_\alpha^R| \end{cases}. \quad (21)$$

Put together, we arrive at the following topological invariant and bulk-edge correspondence of the NHSSH (α, α') chain assuming $0 \leq \alpha < \alpha'$, i.e.,

$$W = \frac{W_1 + W_2}{2} = \begin{cases} \alpha, & |J_\alpha^L J_{\alpha'}^R| \leq |J_{\alpha'}^L J_\alpha^R| \\ \alpha', & |J_\alpha^L J_{\alpha'}^R| > |J_{\alpha'}^L J_\alpha^R| \end{cases}, \quad (22)$$

$$N_0 = 2|W| = \begin{cases} 2\alpha, & |J_\alpha^L J_{\alpha'}^R| \leq |J_{\alpha'}^L J_\alpha^R| \\ 2\alpha', & |J_\alpha^L J_{\alpha'}^R| > |J_{\alpha'}^L J_\alpha^R| \end{cases}. \quad (23)$$

We conclude that the critical points along $|J_\alpha^L J_{\alpha'}^R| = |J_{\alpha'}^L J_\alpha^R|$ are topologically nontrivial whenever $\alpha > 0$. Their nontrivial topologies are characterized by a quantized winding number $W = \alpha$ and a number $N_0 = 2\alpha$ of edge modes coexisting with a gapless bulk at zero energy. Instead, the critical points along $|J_\alpha^L J_{\alpha'}^R| = |J_{\alpha'}^L J_\alpha^R|$ are topologically trivial when $\alpha = 0$, regardless of the value of α' . Away from the critical points, we find two distinct gapped phases with the winding numbers α, α' and the numbers of edge zero modes $2\alpha, 2\alpha'$. These gapped phases and gapless phase boundaries could thus be completely described within our theoretical framework.

We now verify our theory with two sets of computational examples. One of them shows trivial critical points, while the other holds topologically nontrivial critical points with edge zero modes. We first consider the case with $(\alpha, \alpha') = (0, 1)$. The complex-extended Hamiltonian reads $H_{01}(z) \equiv H_0(z) + H_1(z)$. For the hopping parameters, we choose $J_0^L = J - \gamma$, $J_0^R = J + \gamma$ ($J, \gamma \in \mathbb{R}$), and set $J_1^L = J_1^R = 1$ as the unit of energy. This $H_{01}(z)$ is non-Hermitian when $\gamma \neq 0$. The non-Hermiticity is originated from asymmetric intracell hoppings. Following Eqs. (17) and (18), the radius r_0 of GBZ and the phase boundary equation in this case are given by

$$r_0 = \sqrt{|J - \gamma|/|J + \gamma|}, \quad J^2 = \gamma^2 \pm 1. \quad (24)$$

The topological winding number W and the number of zero-energy edge modes N_0 are further predicted by

Eqs. (22) and (23) as

$$W = \begin{cases} 1, & |J^2 - \gamma^2| < 1 \\ 0, & \text{Otherwise} \end{cases}, \quad (25)$$

$$N_0 = \begin{cases} 2, & |J^2 - \gamma^2| < 1 \\ 0, & \text{Otherwise} \end{cases}. \quad (26)$$

We notice that in the limit $\gamma = 0$, the properties of Hermitian SSH model are recovered [93].

These theoretical results can be verified by computing the zero energy solutions of the system explicitly. In the lattice representation, the Hamiltonian of NHSSH (0,1) chain reads $\hat{H}_{01} = \hat{H}_0 + \hat{H}_1$, where $\hat{H}_0 = \sum_n [(J + \gamma)\hat{a}_n^\dagger \hat{b}_n + (J - \gamma)\hat{b}_n^\dagger \hat{a}_n]$ and $\hat{H}_1 = \sum_n (\hat{b}_n^\dagger \hat{a}_{n+1} + \hat{a}_{n+1}^\dagger \hat{b}_n)$. For a chain with unit cell indices $n = 1, 2, \dots, N$ under the OBC, the (non-normalized) zero-energy eigenstates can be found in the limit $N \rightarrow \infty$ as (see Appendix A for details)

$$\begin{aligned} |\psi_0^L\rangle &= \sum_{n=1}^N [-\varrho(J - \gamma)]^{n-1} \hat{a}_n^\dagger |\emptyset\rangle, \\ |\psi_0^R\rangle &= \sum_{n=1}^N [-\varrho^{-1}(J + \gamma)]^{N-n} \hat{b}_n^\dagger |\emptyset\rangle, \end{aligned} \quad (27)$$

where $|\varrho| = \sqrt{|J + \gamma|/|J - \gamma|}$. These states could describe a pair of edge zero modes if and only if $|J^2 - \gamma^2| < 1$ (see also Appendix A), which is exactly the condition for the system to be in its gapped topological phase with the winding number $W = 1$ and the number of zero-energy edge modes $N_0 = 2$, as reported in Eqs. (25) and (26). Our theoretical predictions are thus confirmed. Notably, the edge zero modes $|\psi_0^L\rangle$ and $|\psi_0^R\rangle$ become delocalized at the critical points $J^2 - \gamma^2 = \pm 1$. The gapless phase boundary of the NHSSH (0,1) chain is thus topologically trivial, which is characterized by the winding number $W = 0$ and the number of edge zero modes $N_0 = 0$.

Below, we provide further evidence to testify our theoretical discoveries. Plugging $(J_0^L, J_0^R) = (J - \gamma, J + \gamma)$ and $(J_1^L, J_1^R) = (1, 1)$ into the Eqs. (15) and (16), we find that the $P(z)$ has two zeros at $z = 0, -(J - \gamma)$ and a pole at $z = -1/(J + \gamma)$, while the $Q(z)$ has two zeros at $z = -(J - \gamma), -1/(J + \gamma)$ and a pole at $z = 0$. All these zeros and poles are of order one. In Fig. 4, we show the topological phase diagram of NHSSH (0,1) chain, its GBZ and zero-pole configurations for some typical cases. The phase diagram in Fig. 4(a) has two topologically distinct gapped phases with $W = 0$ and 1. They are separated by four phase boundaries [Eq. (24)], where the two non-Bloch bands of the system touches with each other. Along the dotted parameter line in Fig. 4(a), we pick up five representative points $\bullet, \blacktriangleright, \blacklozenge, \blacktriangleleft, \blacksquare$. The GBZ of the system and the zero/pole locations of the $P(z)$ and

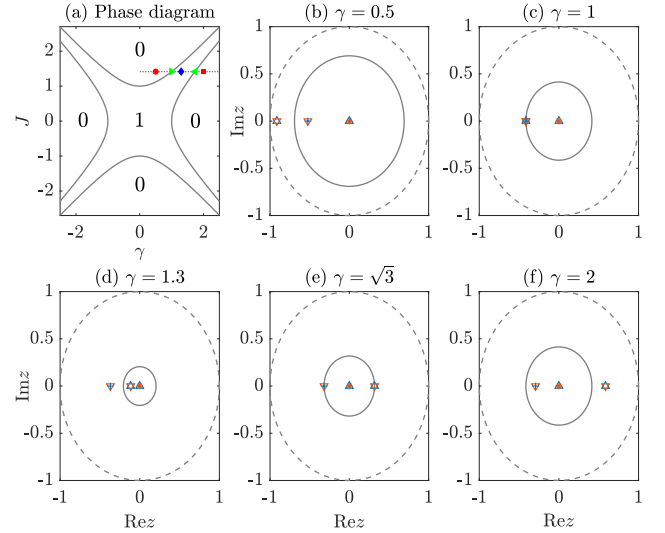


FIG. 4. Phase diagram, GBZ and zero/pole distributions of the NHSSH (0,1) chain. (a) Topological phase diagram, with the values of W shown explicitly in each phase. Phase boundaries are given by the gray solid lines. Along the dotted line, the symbols \bullet , \blacktriangleright , \blacklozenge , \blacktriangleleft , and \blacksquare highlight the points in the parameter space with $J = \sqrt{2}$ and $\gamma = 0.5, 1, 1.3, \sqrt{3}$, and 2, respectively. (b)–(f) show the BZ (in dashed rings), GBZ (in solid rings), zeros of $P(z)$ (in \triangle), poles of $P(z)$ (in $+$), zeros of $Q(z)$ (in ∇), and poles of $Q(z)$ (in $*$) for the five points in (a) from left to right on the complex z -plane, respectively.

$Q(z)$ at these points are shown in Figs. 4(b)–4(f). Our theoretical predictions are clearly verified in each case. For example, in Fig. 4(d), we find two zeros (one zero) of $P(z)$ ($Q(z)$) and one pole of $Q(z)$ inside the GBZ, yielding the winding numbers $W_1 = 2 - 0 = 2$, $W_2 = 1 - 1 = 0$, and thus $W = (W_1 + W_2)/2 = 1$. In Fig. 4(e), we find only a zero of $P(z)$ and a pole of $Q(z)$ inside the GBZ, yielding the winding numbers $W_1 = 1 - 0 = 1$, $W_2 = 0 - 1 = -1$, and $W = (W_1 + W_2)/2 = 0$. This critical point is thus topologically *trivial*. Note in passing that if we only take into account the contribution of $P(z)$ inside the GBZ, as did in previous studies for gapped phases [30], we will obtain $W = W_1 = 1$, leading to the prediction that the critical point at $(J, \gamma) = (\sqrt{2}, \sqrt{3})$ is topologically *nontrivial*! We will soon verify that this prediction is incorrect, as there are no edge zero modes at this critical point. Our work then generalizes previous theories on gapped non-Hermitian topological phases to a rule applicable to both gapped and gapless situations.

In Fig. 5, we present the spectra and edge states of the NHSSH (0,1) chain. In Fig. 5(a), the blue dots correspond to the spectrum obtained under the OBC, whereas the red line describes the spectrum gap $\min_{k \in [-\pi, \pi]} |E(k)|$ obtained under the PBC. It is clear that the PBC and OBC spectra have different gap closing points, which demonstrates the breakdown of Hermitian bulk-edge correspondence and the necessity of incorporating the non-Bloch band theory to characterize the NHSSH (0,1) chain. In the parameter region $\gamma \in (1, \sqrt{3})$,

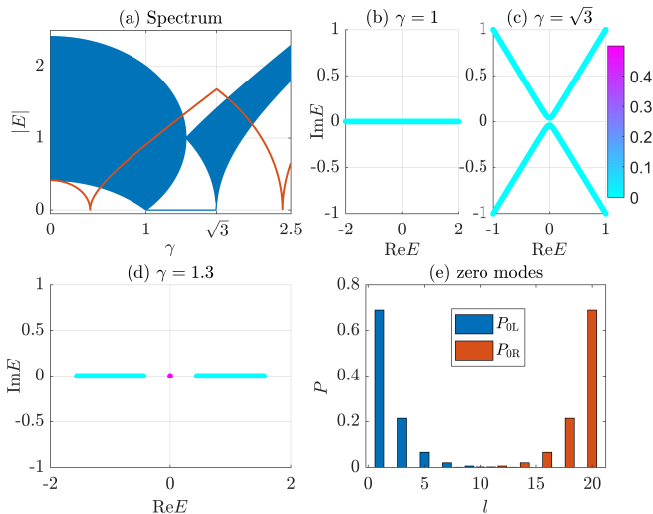


FIG. 5. Spectra and edge states of the NHSSH (0,1) chain with $J = \sqrt{2}$. (a) shows the absolute value of spectrum $|E|$ vs γ under the OBC (in blue dots), with the red curve denoting the magnitude of spectral gap at $E = 0$ under the PBC. (b)–(d) show the spectra at different γ on the complex plane, with the shared color bar giving the inverse participation ratio of each eigenstate. (e) shows the probability distributions P_{0L} and P_{0R} of the two zero modes in (d) for a lattice with 10 unit cells.

we further observe eigenmodes pinned at zero energy, which represent topological edge modes. As illustrated by the OBC spectra in Figs. 5(b) and 5(c), these edge modes are absent at the critical points $\gamma = 1, \sqrt{3}$, which confirms the topological triviality of gap closing (phase transition) points in the NHSSH (0,1) chain. The OBC spectrum at $\gamma = 1.3$ in Fig. 5(d) instead holds a pair of zero modes in the bulk gap, whose spatial profiles are shown in Fig. 5(e). These zero modes are indeed localized at the edges of the lattice, which verifies the prediction of winding number $W = 1$ and number of edge modes $N_0 = 2$ at $(J, \gamma) = (\sqrt{2}, 1.3)$ in the phase diagram Fig. 4(a). Overall, the results presented in Fig. 5 are consistent with our theoretical descriptions, which further affirms the applicability of our approach to the topological characterization of both gapped and gapless phases in sublattice-symmetric non-Hermitian systems.

We next consider the case with $(\alpha, \alpha') = (1, 2)$. The complex-extended Hamiltonian reads $H_{12}(z) \equiv H_1(z) + H_2(z)$. For the hopping parameters, we take $J_1^L = J - \gamma$, $J_1^R = J + \gamma$ ($J, \gamma \in \mathbb{R}$), and let $J_2^L = J_2^R = 1$ be the unit of energy. The $H_{12}(z)$ is also non-Hermitian when $\gamma \neq 0$. The non-Hermiticity is now due to asymmetric intercell hoppings $J_1^{L,R}$. Following Eqs. (17) and (18), the GBZ radius r_0 and phase boundary equation in this case are still given by the Eq. (24). While the topological invariant W and the number of zero-energy edge modes

N_0 are predicted by the Eqs. (22) and (23) as

$$W = \begin{cases} 2, & |J^2 - \gamma^2| < 1 \\ 1, & \text{Otherwise} \end{cases}, \quad (28)$$

$$N_0 = \begin{cases} 4, & |J^2 - \gamma^2| < 1 \\ 2, & \text{Otherwise} \end{cases}. \quad (29)$$

We notice that even though the GBZ radii and phase boundaries of $H_{01}(z)$ and $H_{12}(z)$ are identical, their winding numbers and edge mode configurations are different in each phase. Importantly, the critical points of $H_{12}(z)$ along the phase boundary $J^2 = \gamma^2 \pm 1$ are all topologically nontrivial, characterized by the invariant $W = 1$ and the number of edge zero modes $N_0 = 2$. Despite the point at $\gamma = 0$, these topologically nontrivial critical points are unique to non-Hermitian systems, as the conventional bulk-edge correspondence breaks down at each of these points due to the difference between the BZ and GBZ.

The Eqs. (28) and (29) can also be verified by computing the zero-energy solutions of the system. In the lattice representation, the Hamiltonian of NHSSH (1,2) chain takes the form $\hat{H}_{12} = \hat{H}_1 + \hat{H}_2$, where $\hat{H}_1 = \sum_n [(J - \gamma)\hat{b}_n^\dagger \hat{a}_{n+1} + (J + \gamma)\hat{a}_{n+1}^\dagger \hat{b}_n]$ and $\hat{H}_2 = \sum_n (\hat{b}_n^\dagger \hat{a}_{n+2} + \hat{a}_{n+2}^\dagger \hat{b}_n)$. For a chain with unit cell indices $n = 1, 2, \dots, N$ under the OBC, the (non-normalized) zero-energy eigenstates are found in the limit $N \rightarrow \infty$ as (see Appendix A for details)

$$\begin{aligned} |\varphi_0^{L,1}\rangle &= \hat{a}_1^\dagger |\emptyset\rangle, \\ |\varphi_0^{L,2}\rangle &= \sum_{n=2}^N [-\varrho(J - \gamma)]^{n-2} \hat{a}_n^\dagger |\emptyset\rangle, \\ |\varphi_0^{R,1}\rangle &= \hat{b}_N^\dagger |\emptyset\rangle, \\ |\varphi_0^{R,2}\rangle &= \sum_{n=1}^{N-1} [-\varrho^{-1}(J + \gamma)]^{N-n-1} \hat{b}_n^\dagger |\emptyset\rangle, \end{aligned} \quad (30)$$

where $|\varrho| = \sqrt{|J + \gamma|/|J - \gamma|}$. The eigenmodes $|\varphi_0^{L,1}\rangle$ and $|\varphi_0^{L,2}\rangle$ persist at the two ends of the chain throughout the parameter space. They could thus survive at the critical points $J^2 = \gamma^2 \pm 1$, making the latter topologically nontrivial with $W = 1$ and the number of edge zero modes $N_0 = 2$. Meanwhile, the states $|\varphi_0^{L,2}\rangle$ and $|\varphi_0^{R,2}\rangle$ form a pair of edge zero modes if and only if $|J^2 - \gamma^2| < 1$ (see Appendix A for details). Therefore, they could only survive in the gapped phase of the chain with $W = 2$ and the number of edge zero modes $N_0 = 4$, as described by the Eqs. (28) and (29). In the region $|J^2 - \gamma^2| > 1$, we are left with the edge zero modes $|\varphi_0^{L,1}\rangle$ and $|\varphi_0^{R,2}\rangle$, which is coincident with the gapped topological phase of $W = 1$ and $N_0 = 2$ according to the Eqs. (28) and (29). These observations confirm that our theory is valid in both the

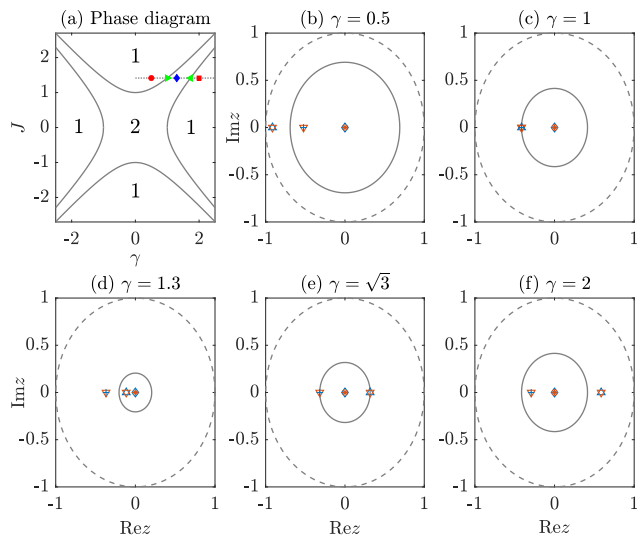


FIG. 6. Phase diagram, GBZ and zero/pole distributions of the NHSSH (1, 2) chain. (a) Topological phase diagram, with the values of W shown explicitly in each phase. Phase boundaries are given by the gray solid lines. Along the dotted line, the symbols \bullet , \blacktriangleright , \blacklozenge , \blacktriangleleft , and \blacksquare highlight the points in the parameter space with $J = \sqrt{2}$ and $\gamma = 0.5, 1, 1.3, \sqrt{3}$, and 2 , respectively. (b)–(f) show the BZ (in dashed rings), GBZ (in solid rings), zeros of $P(z)$ (in \diamond and \triangle for the third order and first order ones), poles of $P(z)$ (in $+$), zeros of $Q(z)$ (in ∇), and poles of $Q(z)$ (in $*$) for the five exemplary points in (a) from left to right on the complex z -plane.

gapped topological phases and along the gapless phase boundaries of the NHSSH (1, 2) chain. Importantly, the nontrivial critical points of non-Bloch bands are correctly depicted within our topological characterization.

In the rest of this subsection, we offer additional evidence to support our findings. Inserting $(J_1^L, J_1^R) = (J - \gamma, J + \gamma)$ and $(J_2^L, J_2^R) = (1, 1)$ into the Eqs. (15) and (16), we realize that the $P(z)$ has two zeros at $z = 0$ (order 3), $z = -(J - \gamma)$ (order 1), and a pole at $z = -1/(J + \gamma)$ (order 1). The $Q(z)$ has two zeros at $z = -(J - \gamma)$, $-1/(J + \gamma)$ and a pole at $z = 0$. The zeros and poles of $Q(z)$ are all of order one. In Fig. 6, we show the topological phase diagram of our NHSSH (1, 2) chain, its GBZ and zero/pole locations for typical cases. We notice that the phase boundaries in Figs. 4(a) and 6(a) have the same configurations, as described by the Eq. (24). Nevertheless, the invariant W of their corresponding phases are different, and the gapped phases of NHSSH (1, 2) chain are all topologically nontrivial. In Fig. 6(a), we take the same representative points at \bullet , \blacktriangleright , \blacklozenge , \blacktriangleleft , and \blacksquare as in Fig. 4(a), and show their respective GBZ and zero/pole distributions of $P(z)$ and $Q(z)$ in Fig. 6(b)–(f). The results are again consistent with our predictions in each case. Different from the (0, 1) chain, the critical points of the (1, 2) chain at $(J, \gamma) = (\sqrt{2}, 1)$ [Fig. 6(c)] and $(J, \gamma) = (\sqrt{2}, \sqrt{3})$ [Fig. 6(e)] (and along other phase boundaries) are found to be topologically nontrivial. For example, at $(J, \gamma) = (\sqrt{2}, \sqrt{3})$ in

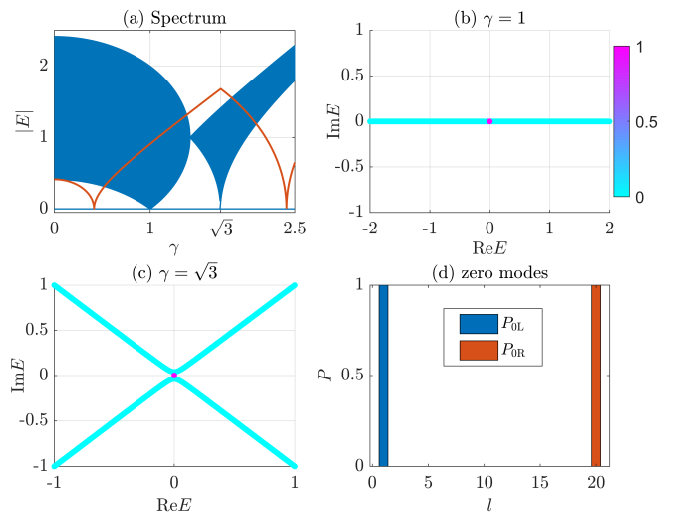


FIG. 7. Spectra and edge states of the NHSSH (1, 2) chain with $J = \sqrt{2}$. (a) shows the absolute value of spectrum $|E|$ vs γ under the OBC (in blue dots), with the red curve denoting the magnitude of spectral gap at $E = 0$ under the PBC. (b) and (c) show the spectra at $\gamma = 1$ and $\sqrt{3}$ on the complex plane, with the shared color bar giving the inverse participation ratio of each eigenstate. (d) shows the probability distributions P_{0L} and P_{0R} of the two zero modes in (b) for a lattice with 10 unit cells. The two edge modes in (c) have the same profiles P_{0L} and P_{0R} .

Fig. 6(a), we have $W_1 = 3 - 0 = 3$ and $W_2 = 0 - 1 = -1$ for the $P(z)$ and $Q(z)$ in Fig. 6(e), yielding the invariant $W = (W_1 + W_2)/2 = 1$. We will demonstrate that there is indeed a number of $N_0 = 2|W| = 2$ edge zero modes at this critical point, verifying our prediction in Eq. (29). It deserves to emphasize again that taking only the zero/pole contribution of $P(z)$ into account will lead to $W = W_1 = 3$, which could not generate any reliable predictions about the numbers of edge zero modes that could appear at the critical point.

In Fig. 7, we present the spectra and edge states of the NHSSH (1, 2) chain. We observe that under the OBC, zero energy eigenmodes persist throughout the spectrum (blue dots) in Fig. 7(a). Meanwhile, the gap closing points under the PBC and OBC are again different, making it necessary to employ the non-Bloch band theory for topological characterizations. Notably, we observe strongly localized zero modes in the spectra at the critical points $(J, \gamma) = (\sqrt{2}, 1)$ and $(\sqrt{2}, \sqrt{3})$, as presented in Figs. 7(b) and 7(c). It implies that in stark contrast to the NHSSH (0, 1) chain, the band touching points of NHSSH (1, 2) chain are topologically nontrivial. Indeed, the zero modes in Figs. 7(b) and 7(c) are both localized at the two ends of the chain, forming a pair of degenerate edge modes at $E = 0$ as shown in Fig. 7(d). On the other hand, our bulk theory yields the winding number $W = 1$ at both critical points, leading to the consistent bulk-edge correspondence $N_0 = 2|W|$. Therefore, beyond previous approaches, our theory allows us to identify a unique class of topologically nontrivial gapless points be-

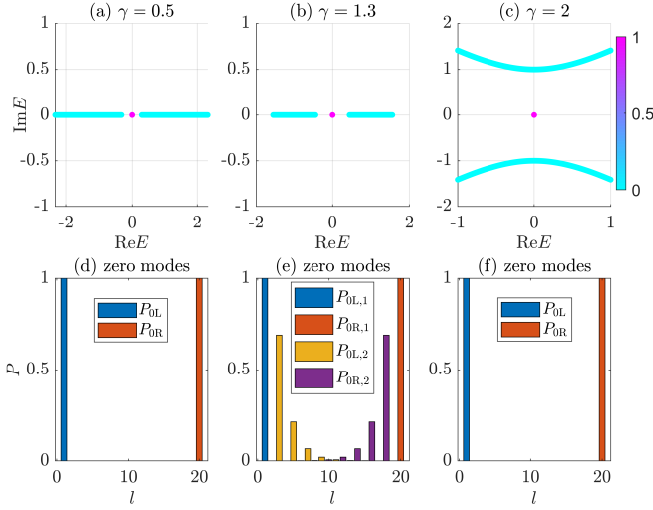


FIG. 8. Spectra and edge states of the NHSSH (1,2) chain with $J = \sqrt{2}$ for three gapped phases. In (a), there are two edge zero modes, whose probability distributions P_{0L} and P_{0R} are shown in (d) for a lattice with 10 unit cells. In (b), there are four edge zero modes, whose probability distributions $P_{0L,1}$, $P_{0R,1}$, $P_{0L,2}$ and $P_{0R,2}$ are presented in (e) for a lattice with 10 unit cells. In (c), there are two edge zero modes, whose probability distributions P_{0L} and P_{0R} are given in (f) for a lattice with 10 unit cells.

tween non-Bloch bands and characterize the associated bulk-edge correspondence in 1D non-Hermitian systems.

For completeness, we present the spectra and edge states of the NHSSH (1,2) chain for three gapped phases in Fig. 8, whose system parameters are given by $(J, \gamma) = (\sqrt{2}, 0.5)$, $(\sqrt{2}, 1.3)$ and $(\sqrt{2}, 2)$ in the phase diagram Fig. 6(a). According to the phase diagram, the topological invariants of these phases are $W = 1, 2, 1$, while the numbers of edge zero modes in Figs. 8(d)–8(f) are $N_0 = 2, 4, 2$. The bulk-edge correspondence $N_0 = 2|W|$ is thus verified for these gapped phases. In conclusion, we have demonstrated the applicability of our theory to the topological characterization of NHSSH (α, α') chains for both gapped and gapless phases. In the next subsection, we study a more complicated class of NHSSH chain and reveal the presence of phase transitions along topological phase boundaries therein.

D. $(\alpha, \alpha', \alpha'')$ chain: critical topological phase transitions

As a final example, we consider a NHSSH chain with three hopping ranges. Extending e^{ik} to the whole complex plane, the Hamiltonian of such a NHSSH $(\alpha, \alpha', \alpha'')$ chain reads $H(z) = H_\alpha(z) + H_{\alpha'}(z) + H_{\alpha''}(z)$ where $\alpha \neq \alpha' \neq \alpha''$. To simplify the analytical treatments and pinpoint the key physics, we focus on the case with $\alpha \geq 0$, $\alpha' = \alpha + 1$ and $\alpha'' = \alpha + 2$. Under these assumptions, we find the characteristic functions $P(z)$ and $Q(z)$

of NHSSH $(\alpha, \alpha + 1, \alpha + 2)$ chain as

$$P(z) = z^{2\alpha+2} \frac{J_{\alpha+2}^L z^2 + J_{\alpha+1}^L z + J_\alpha^L}{J_\alpha^R z^2 + J_{\alpha+1}^R z + J_{\alpha+2}^R}, \quad (31)$$

$$Q(z) = \frac{(J_{\alpha+2}^L z^2 + J_{\alpha+1}^L z + J_\alpha^L)(J_\alpha^R z^2 + J_{\alpha+1}^R z + J_{\alpha+2}^R)}{z^2}. \quad (32)$$

It can be verified that the $P(z)$ has a zero of order $2\alpha + 2$ at $z = 0$, two other zeros of order one at

$$z_\pm^L = \frac{-J_{\alpha+1}^L \pm \sqrt{(J_{\alpha+1}^L)^2 - 4J_\alpha^L J_{\alpha+2}^L}}{2J_{\alpha+2}^L}, \quad (33)$$

and two poles of order one at

$$z_\pm^R = \frac{-J_{\alpha+1}^R \pm \sqrt{(J_{\alpha+1}^R)^2 - 4J_\alpha^R J_{\alpha+2}^R}}{2J_\alpha^R}. \quad (34)$$

Meanwhile, the $Q(z)$ has for zeros of order one at $z_\pm^{L,R}$ and a pole of order two at $z = 0$. The locations of these zeros and poles versus the GBZ determine the topological invariants of the system following Eqs. (6) and (7).

To proceed, we need to obtain the GBZ from the two middle solutions of the equation $Q(z) = Q(ze^{i\theta})$ for $\theta \in [0, 2\pi]$ [26]. As a further simplification, we take $J_\beta^L = J_\beta^R = J_\beta \in \mathbb{C}$ with $\beta = \alpha, \alpha + 1, \alpha + 2$ for the hopping amplitudes and set $J_{\alpha+1} = 1$ as the unit of energy. The system Hamiltonian remains non-Hermitian whenever there exists a $\beta \in \{\alpha, \alpha + 1, \alpha + 2\}$ such that $J_\beta \neq J_\beta^*$. Substituting these conditions into the equation $Q(z) = Q(ze^{i\theta})$, we obtain

$$(J_{\alpha+2} + J_\alpha)ze^{i\theta} + J_\alpha J_{\alpha+2}(e^{i\theta} + 1) = J_\alpha J_{\alpha+2} z^4 e^{i2\theta}(e^{i\theta} + 1) + (J_{\alpha+2} + J_\alpha)z^3 e^{i2\theta}. \quad (35)$$

For each given set of parameters $(J_\alpha, J_{\alpha+2}, \theta)$, this equation has four solutions in z , with two of them given by $z_\pm = \pm e^{-i\theta/2}$. As these solutions have equal magnitudes $|z_+| = |z_-| = 1$, they must be the two middle solutions that determine the GBZ of the system. Therefore, the GBZ radius is given by $r_0 = |z_\pm| = 1$, which means that it is identical to the standard BZ. Nevertheless, we will show that there are also topological phases and transitions induced by non-Hermitian effects, which are captured by our theoretical framework.

In Fig. 9, we show the topological phase diagram of NHSSH $(\alpha, \alpha + 1, \alpha + 2)$ chain for a representative case. Each continuous region with a uniform color corresponds to a gapped phase, while the red dashed and dotted lines depict topological phase boundaries. In the region surrounded by the red dashed lines, we have $|z_\pm^L| > 1$ and $|z_\pm^R| < 1$. The winding numbers of $P(z)$ and $Q(z)$ are thus given by $W_1 = 2\alpha$ and $W_2 = 0$, yielding the topological invariant $W = \alpha$ for the corresponding phase. In the region sandwiched between the red dashed and

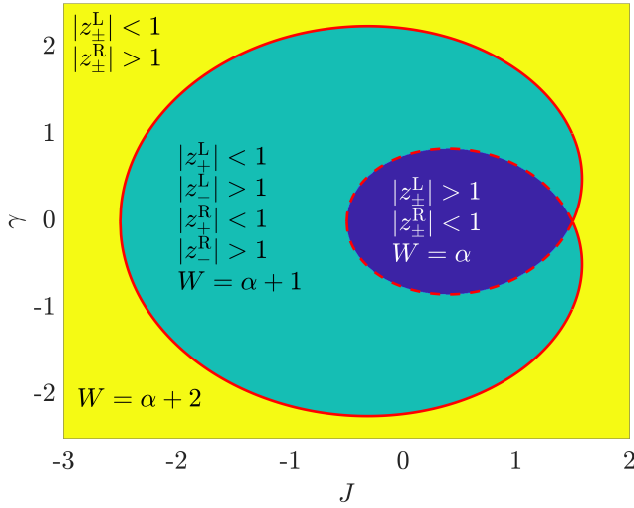


FIG. 9. Topological phase diagram of the NHSSH ($\alpha, \alpha + 1, \alpha + 2$) chain. System parameters are $J_\alpha^L = J_\alpha^R = J_\alpha = 1.5$, $J_{\alpha+1}^L = J_{\alpha+1}^R = J_{\alpha+1} = 1$ and $J_{\alpha+2}^L = J_{\alpha+2}^R = J_{\alpha+2} = J + i\gamma$, where $J, \gamma \in \mathbb{R}$. Each region with a uniform color refers to a gapped phase, with its topological invariant W and zero/pole locations $|z_\pm^L|, |z_\pm^R|$ relative to GBZ shown explicitly therein. The red dashed and solids lines correspond to two sets of topologically distinct phase boundaries with $W = \alpha$ and $W = \alpha + 1$, respectively.

solid lines, we have $|z_+^L| < 1$, $|z_-^L| > 1$, $|z_+^R| < 1$ and $|z_-^R| > 1$. The winding numbers of $P(z)$ and $Q(z)$ are thus given by $W_1 = 2\alpha + 2$ and $W_2 = 0$, leading to the topological invariant $W = \alpha + 1$ for this phase. In the region outside the red solid lines, we have $|z_\pm^L| < 1$ and $|z_\pm^R| > 1$. The winding numbers of $P(z)$ and $Q(z)$ are then given by $W_1 = 2\alpha + 4$ and $W_2 = 0$, generating the topological invariant $W = \alpha + 2$ for the associated phase. The red dashed line in Fig. 9 is given by the solution of $|z_+^L| = |z_+^R| = 1$. On this dashed line, we have $|z_-^L| > 1$ and $|z_+^R| < 1$. Therefore, along the phase boundary depicted by the red dashed line, we find the winding numbers of $P(z)$ and $Q(z)$ as $W_1 = 2\alpha + 1$ and $W_2 = -1$, yielding the topological invariant $W = \alpha$. We conclude that the red dashed critical line in Fig. 9 is topologically trivial (nontrivial) if $\alpha = 0$ ($\alpha > 0$). On the other hand, the red solid line in Fig. 9 is given by the solution of $|z_-^L| = |z_+^R| = 1$. On this solid line, we find $|z_+^L| < 1$ and $|z_-^R| > 1$. Therefore, along the phase boundary depicted by the red solid line, the winding numbers of $P(z)$ and $Q(z)$ are $W_1 = 2\alpha + 3$ and $W_2 = -1$, yielding the topological invariant $W = \alpha + 1$. We conclude that the red solid critical line in Fig. 9 is topologically nontrivial for all $\alpha \geq 0$.

Up to now, we have achieved the topological characterization of all gapped phases and gapless phase boundaries for our considered NHSSH ($\alpha, \alpha + 1, \alpha + 2$) chain. Two additional points deserve to be mentioned. First, by increasing the strength of non-Hermitian parameter γ , we could obtain phases with enlarged topological invariants

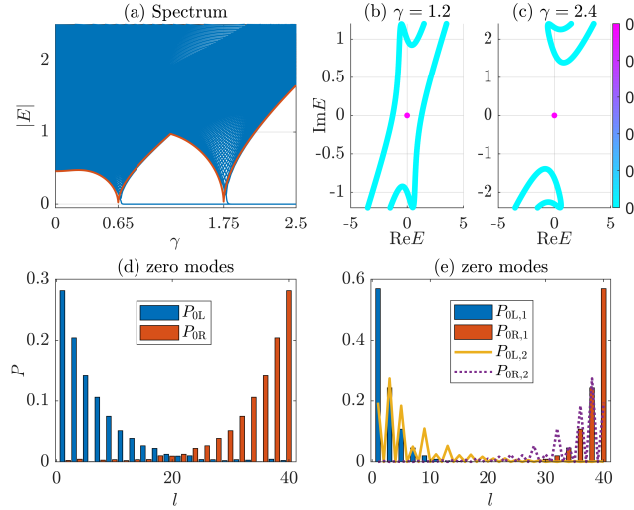


FIG. 10. Spectra and edge states of the NHSSH ($\alpha, \alpha + 1, \alpha + 2$) chain with $\alpha = 0$, $J_\alpha^L = J_\alpha^R = J_\alpha = 1.5$, $J_{\alpha+1}^L = J_{\alpha+1}^R = J_{\alpha+1} = 1$, $J_{\alpha+2}^L = J_{\alpha+2}^R = J_{\alpha+2} = J + i\gamma$ and $J = 1$. (a) shows the absolute value of spectrum $|E|$ vs γ under the OBC (in blue dots), with the red curve denoting the magnitude of spectral gap at $E = 0$ under the PBC. (b) and (c) show the spectra at $\gamma = 1.2$ and 2.4 on the complex plane, with the shared color bar giving the inverse participation ratio of each eigenstate. (d) shows the probability distributions P_{0L} and P_{0R} of the two zero modes in (b) for a lattice with 20 unit cells. (e) shows the probability distributions $P_{0L,1}$, $P_{0R,1}$, $P_{0L,2}$ and $P_{0R,2}$ of the four zero modes in (c) for a lattice with 20 unit cells.

($W = \alpha \rightarrow \alpha + 1 \rightarrow \alpha + 2$) and thus enriched topological signatures. These non-Hermiticity induced topological properties are fully captured by our theory. Second, by changing the system parameter $J_{\alpha+2} = J + i\gamma$ across the multicritical point $(J, \gamma) = (1.5, 0)$ smoothly from the red dashed to solid lines, we will encounter a topological phase transition with the W going from α to $\alpha + 1$. This transition does not require the closing and reopening of any bulk spectral gaps at zero energy. Therefore, we could have a phase transition along topologically distinct gapless phase boundaries in the NHSSH ($\alpha, \alpha + 1, \alpha + 2$) chain. The topological character of such a transition is again well described by our approach, while existing theories developed for gapped non-Hermitian phases (either with point or line gaps) fail to do so.

We next illustrate our results about the NHSSH ($\alpha, \alpha + 1, \alpha + 2$) chain with numerical examples. To be explicit, we focus on the case with $\alpha = 0$, set the second neighbor hopping $J_2 = J + i\gamma$ as the complex parameter, and fix other system parameters as $(J_0, J_1, J) = (1.5, 1, 1)$. The resulting energy spectrum is shown in Fig. 10(a). With the increase of γ , we observe two phase transitions accompanied by the closing/reopening of bulk spectral gaps (highlighted by the red solid line) at $\gamma \approx 0.65$ and $\gamma \approx 1.75$. After each transition, more eigenmodes appear in the spectrum under the OBC (blue dots) at zero energy. These zero modes are spatially localized, as exem-

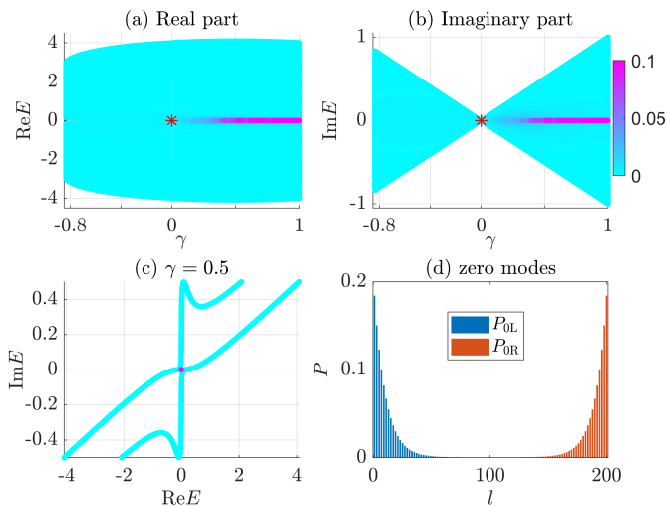


FIG. 11. Spectra and edge states of the NHSSH $(\alpha, \alpha + 1, \alpha + 2)$ chain along the critical line. We set $\alpha = 0$, $J_\alpha^L = J_\alpha^R = J_\alpha = 1.5$, $J_{\alpha+1}^L = J_{\alpha+1}^R = J_{\alpha+1} = 1$, and $J_{\alpha+2}^L = J_{\alpha+2}^R = J_{\alpha+2} = J + i\gamma$. In (a) and (b), the values of J and γ are taken along the red dashed (solid) line in Fig. 9 with $J \in [0.5, 1.5]$ ($\gamma \in (0, 1]$) for $\gamma \leq 0$ ($\gamma > 0$). (a) and (b) show the real and imaginary parts of the spectrum under the OBC, where the red stars highlight the location of multicritical point at $(J, \gamma) = (1.5, 0)$, and the color of each data point gives the inverse participation ratio of the corresponding state. (c) shows the spectrum at $\gamma = 0.5$ in (a) and (b) on the complex plane. (a)–(c) share the same color bar. (d) shows the probability distributions of the two critical edge modes at $E = 0$ in (c) for a lattice with 100 unit cells.

plified by their inverse participation ratios in the spectra reported in Figs. 10(b) and 10(c) for $\gamma = 1.2$ and 2.4, respectively. These zero modes are also found to stay at the two edges of the system, as shown in Figs. 10(d) and 10(f). Further counting reveals that with the raise of γ , the number of edge zero modes we obtained following the two sequential topological transitions are $N_0 = 2$ and 4. Meanwhile, according to the phase diagram Fig. 9, the three gapped phases in Fig. 10(a) from left to right have the topological invariants $W = 0, 1$ and 2, successively. The bulk-edge correspondence $N_0 = 2|W|$, as predicted by our theory, is thus verified for all gapped phases of the NHSSH $(\alpha, \alpha + 1, \alpha + 2)$ chain with $\alpha = 0$. We have also checked and confirmed that other choices of $\alpha > 0$ generate consistent results.

Finally, we demonstrate the emergence of critical edge states following phase transitions along non-Hermitian topological phase boundaries in Fig. 11. We focus on a parameter path in Fig. 9 along the dashed critical line with $J \in [0.5, 1.5]$ for $\gamma \leq 0$, followed by the solid critical line with $\gamma \in (0, 1]$ for $\gamma > 0$. These two critical lines, which have been identified as topologically distinct according to our theory, are interconnected at the multicritical point $(J, \gamma) = (1, 0)$ in Fig. 9. Interestingly, we observe that by passing through the multicritical point from the dashed to solid phase boundaries, localized eigen-

modes are generated at zero energy without undergoing any gap closing and reopening processes in the complex spectrum, as presented in Figs. 11(a) and 11(b). Moreover, the emerging zero modes are indeed coexistent with a gapless bulk and localized spatially around the two ends of the lattice, as shown in Figs. 11(c) and 11(d). These zero modes are thus referred to as non-Hermitian critical edge states, whose topological origin following the “*phase transition of phase transition*” along the gapless critical line is well described by our theory. Indeed, the phase diagram reported in Fig. 9 predicts $W = 0$ and $W = 1$ along the dashed and solid phase boundaries. The bulk-edge correspondence $N_0 = 2|W|$ is then verified not only in gapped phases, but also along all gapless phase boundaries of the NHSSH $(\alpha, \alpha + 1, \alpha + 2)$ chain. Following our definition of topological invariant W , we could now arrive at a consistent description of topological phases and transitions in 1D, two-band, sublattice-symmetric non-Hermitian systems. This is regardless of whether the bulk spectrum is gapped or gapless, or whether the underlying Brillouin zone is in Bloch or generalized non-Bloch forms.

IV. SUMMARY AND DISCUSSION

In this work, we revealed and characterized non-Hermiticity induced critical edge states and topologically nontrivial phase transition points in 1D non-Hermitian systems with sublattice symmetry. By applying the Cauchy’s argument principle to two characteristic functions of a non-Hermitian two-band Hamiltonian, we obtain a pair of winding numbers, whose combination yields an integer-quantized topological invariant W . The applicability of this proposed invariant to the overall depiction of gapped topological phases, gapless phase boundaries, topological phase transitions and bulk-edge correspondence is demonstrated by investigating a broad class of non-Hermitian SSH models. Notably, we identify a phase transition induced by non-Hermitian effects along topological phase boundaries, which is accompanied by the quantized jump of our proposed invariant W and the emergence of critical edge zero modes. The origin of these nontrivial gapless topologies could not be consistent described by existing approaches relying on the presence of point or line spectral gaps. One key advantage of our theoretical approach lies in its generality, in the sense that it does not concern whether the bulk bands are separated from edge states of the system by gaps, and whether the underlying band theory is in Bloch or non-Bloch forms. Therefore, we expect our theory to be applicable to the topological characterization of phases and transitions in other more complicated non-Hermitian, two-band models in one dimension with sublattice symmetries.

In future work, it would be interesting to consider the generalization of our theory to systems with more than two bulk bands, in other symmetry classes and beyond one spatial dimension. The extension of our theory to

driven systems would also be of great importance for revealing gapless Floquet topology [76–78] beyond Hermitian limits. Finally, the realization of our NHSSH (0, 1, 2) chain in quantum simulators like electrical, photonic and acoustic systems may lead to the first experimental observation of critical edge modes and topologically nontrivial critical points in non-Hermitian systems, which deserve more thorough explorations.

ACKNOWLEDGMENTS

This work is supported by the National Natural Science Foundation of China (Grants No. 12275260 and No. 11905211), the Fundamental Research Funds for the Central Universities (Grant No. 202364008), and the Young Talents Project of Ocean University of China.

Appendix A: Calculation of the edge states

In this Appendix, we compute the edge modes analytically and determine their existent conditions for NHSSH (α, α') chains with $(\alpha, \alpha') = (0, 1)$ and $(1, 2)$.

In lattice representation, the Hamiltonian of NHSSH (0, 1) chain in Sec. III C takes the form

$$\begin{aligned} \hat{H}_{01} = & \sum_{n \in \mathbb{Z}} \left[(J + \gamma) \hat{a}_n^\dagger \hat{b}_n + (J - \gamma) \hat{b}_n^\dagger \hat{a}_n \right] \\ & + \sum_{n \in \mathbb{Z}} \left(\hat{b}_n^\dagger \hat{a}_{n+1} + \hat{a}_{n+1}^\dagger \hat{b}_n \right). \end{aligned} \quad (\text{A1})$$

Following Ref. [25], we apply the similarity transformation \hat{S} to \hat{H}_{01} under the OBC, where

$$\hat{S} = \sum_{n \in \mathbb{Z}} \left(\varrho^{n-1} \hat{a}_n^\dagger \hat{a}_n + \varrho^n \hat{b}_n^\dagger \hat{b}_n \right). \quad (\text{A2})$$

ϱ is a control parameter. The transformed Hamiltonian takes the form $\hat{H}'_{01} = \hat{S} \hat{H}_{01} \hat{S}^{-1}$, where

$$\begin{aligned} \hat{H}'_{01} = & \sum_{n \in \mathbb{Z}} \left[\varrho^{-1} (J + \gamma) \hat{a}_n^\dagger \hat{b}_n + \varrho (J - \gamma) \hat{b}_n^\dagger \hat{a}_n \right] \\ & + \sum_{n \in \mathbb{Z}} \left(\hat{b}_n^\dagger \hat{a}_{n+1} + \hat{a}_{n+1}^\dagger \hat{b}_n \right). \end{aligned} \quad (\text{A3})$$

We choose ϱ to ensure the left and right intracell hoppings to have equal magnitudes, which means that $|\rho| = \sqrt{|J + \gamma|/|J - \gamma|}$. Let us consider a chain with unit cell indices $n = 1, 2, \dots, N$ and take the OBC at both ends. A zero-energy eigenmode of \hat{H}'_{01} satisfies $\hat{H}'_{01} |\psi_0\rangle = 0$. Expanding $|\psi_0\rangle$ in the lattice representation as $|\psi_0\rangle = \sum_m \left(A_m \hat{a}_m^\dagger + B_m \hat{b}_m^\dagger \right) |\emptyset\rangle$ ($|\emptyset\rangle$ denotes the vacuum state) and applying \hat{H}'_{01} to it, we arrive at the iteration equa-

tions of wave amplitudes (A_n, B_n) , i.e.,

$$\varrho^{-1} (J + \gamma) B_1 = 0, \quad \varrho (J - \gamma) A_N = 0, \quad (\text{A4})$$

$$\varrho (J - \gamma) A_n + A_{n+1} = 0, \quad n = 1, \dots, N - 1, \quad (\text{A5})$$

$$\varrho^{-1} (J + \gamma) B_{n+1} + B_n = 0, \quad n = 1, \dots, N - 1. \quad (\text{A6})$$

In the limit $N \rightarrow \infty$, this set of difference equation has two zero-energy solutions. Their wave functions (up to normalization factors) are given by

$$\begin{aligned} |\psi_0^{\text{L}}\rangle &= \sum_{n=1}^N [-\varrho (J - \gamma)]^{n-1} \hat{a}_n^\dagger |\emptyset\rangle, \\ |\psi_0^{\text{R}}\rangle &= \sum_{n=1}^N [-\varrho^{-1} (J + \gamma)]^{N-n} \hat{b}_n^\dagger |\emptyset\rangle. \end{aligned} \quad (\text{A7})$$

It is clear that the states $|\psi_0^{\text{L}}\rangle$ and $|\psi_0^{\text{R}}\rangle$ represent a left-localized and right-localized edge zero modes if and only if $|\varrho (J - \gamma)| < 1$ and $|(J + \gamma)/\varrho| < 1$, respectively. Both these conditions yield $|J^2 - \gamma^2| < 1$, which is exactly the condition for us to have topologically nontrivial gapped phases with the winding number $W = 1$ and the number of zero-energy edge modes $N_0 = 2$, as reported in Eqs. (25) and (26). The bulk-edge correspondence of our NHSSH (0, 1) chain is thus proved. Importantly, we find no zero-energy edge modes when $J^2 - \gamma^2 = \pm 1$, i.e., at the critical points of the system under the OBC. This observation confirms that the gapless phase boundary of the NHSSH (0, 1) chain is indeed topologically trivial from the perspective of critical edge states.

We next consider the NHSSH (1, 2) chain in Sec. III C, whose Hamiltonian takes the form

$$\begin{aligned} \hat{H}_{12} = & \sum_{n \in \mathbb{Z}} \left[(J - \gamma) \hat{b}_n^\dagger \hat{a}_{n+1} + (J + \gamma) \hat{a}_{n+1}^\dagger \hat{b}_n \right] \\ & + \sum_{n \in \mathbb{Z}} \left(\hat{b}_n^\dagger \hat{a}_{n+2} + \hat{a}_{n+2}^\dagger \hat{b}_n \right). \end{aligned} \quad (\text{A8})$$

Under the similarity transformation

$$\hat{R} = \sum_{n \in \mathbb{Z}} \left(\varrho^{n-1} \hat{a}_n^\dagger \hat{a}_n + \varrho^{n+1} \hat{b}_n^\dagger \hat{b}_n \right), \quad (\text{A9})$$

the \hat{H}_{12} becomes $\hat{H}'_{12} = \hat{R} \hat{H}_{12} \hat{R}^{-1}$, or

$$\begin{aligned} \hat{H}'_{12} = & \sum_{n \in \mathbb{Z}} \left[\varrho (J - \gamma) \hat{b}_n^\dagger \hat{a}_{n+1} + \varrho^{-1} (J + \gamma) \hat{a}_{n+1}^\dagger \hat{b}_n \right] \\ & + \sum_{n \in \mathbb{Z}} \left(\hat{b}_n^\dagger \hat{a}_{n+2} + \hat{a}_{n+2}^\dagger \hat{b}_n \right). \end{aligned} \quad (\text{A10})$$

We choose ϱ to let the left and right intracell hoppings to have equal magnitudes, which again leads to $|\rho| = \sqrt{|J + \gamma|/|J - \gamma|}$. For a chain with unit cell indices $n =$

1, 2, ..., N and under the OBC at both ends, a zero-energy solution of \hat{H}'_{12} satisfies $\hat{H}'_{12}|\varphi_0\rangle = 0$. It is not hard to notice that one set of solutions of this equation is given by the eigenmodes

$$|\varphi_0^{L,1}\rangle = \hat{a}_1^\dagger|\emptyset\rangle, \quad |\varphi_0^{R,1}\rangle = \hat{b}_N^\dagger|\emptyset\rangle, \quad (\text{A11})$$

which form a pair of degenerate edge modes at the left and right ends of the lattice. To find other possible solutions, we again expand the zero mode in the lattice space as $|\varphi_0\rangle = \sum_m (C_m \hat{a}_m^\dagger + D_m \hat{b}_m^\dagger)|\emptyset\rangle$ and apply the Hamiltonian \hat{H}'_{12} to it. The resulting zero-energy solutions in the limit $N \rightarrow \infty$ are given by

$$\begin{aligned} |\varphi_0^{L,2}\rangle &= \sum_{n=2}^N [-\varrho(J - \gamma)]^{n-2} \hat{a}_n^\dagger |\emptyset\rangle, \\ |\varphi_0^{R,2}\rangle &= \sum_{n=1}^{N-1} [-\varrho^{-1}(J + \gamma)]^{N-n-1} \hat{b}_n^\dagger |\emptyset\rangle. \end{aligned} \quad (\text{A12})$$

The states $|\varphi_0^{L,2}\rangle$ and $|\varphi_0^{R,2}\rangle$ represent left-localized and right-localized eigenmodes if and only if $|\varrho(J - \gamma)| < 1$ and $|\varrho^{-1}(J + \gamma)| < 1$, respectively, yielding the condition $|J^2 - \gamma^2| < 1$ for their existence. This is the same condition for us to have topologically nontrivial gapped phases with the winding number $W = 2$ and the number of edge zero modes $N_0 = 4$, as reported in Eqs. (28) and (29). Since the edge modes $|\varphi_0^{L,1}\rangle$ and $|\varphi_0^{R,1}\rangle$ are persistent under this condition, the bulk-edge correspondence of the $W = 2$ phase is confirmed. When $|J^2 - \gamma^2| > 1$, the edge zero modes $|\varphi_0^{L,2}\rangle$ and $|\varphi_0^{R,2}\rangle$ disappear, while the modes $|\varphi_0^{L,1}\rangle$ and $|\varphi_0^{R,1}\rangle$ are retained. This conforms to our expectation for the other gapped topological phase with the winding number $W = 1$ and the number of edge zero modes $N_0 = 2$, as shown in Eqs. (28) and (29). Finally, we notice that the edge modes $|\varphi_0^{L,1}\rangle$ and $|\varphi_0^{R,1}\rangle$ survive at the critical points $|J^2 - \gamma^2| = 1$. Therefore, the phase boundary of the NHSSH (1, 2) chain is topologically nontrivial, which is characterized by a quantized winding number $W = 1$ and a pair of edge modes degenerating with a gapless bulk at zero energy.

-
- [1] V. M. Martinez Alvarez, J. E. Barrios Vargas, M. Berdakin, and L. E. F. Foa Torres, Topological states of non-Hermitian systems, *Eur. Phys. J. Spec. Top.* **227**, 1295–1308 (2018).
- [2] R. El-Ganainy, K. G. Makris, M. Khajavikhan, Z. H. Musslimani, S. Rotter, and D. N. Christodoulides, Non-Hermitian physics and PT symmetry, *Nat. Phys.* **14**, 11–19 (2018).
- [3] Ş. K. Özdemir, S. Rotter, F. Nori, and L. Yang, Parity-time symmetry and exceptional points in photonics, *Nat. Mater.* **18**, 783–798 (2019).
- [4] A. Ghatak and T. Das, New topological invariants in non-Hermitian systems, *J. Phys.: Condens. Matter* **31**, 263001 (2019).
- [5] Y. Ashida, Z. Gong, and M. Ueda, Non-Hermitian physics, *Adv. Phys.* **69**, 249–435 (2020).
- [6] E. J. Bergholtz, J. C. Budich, and F. K. Kunst, Exceptional topology of non-Hermitian systems, *Rev. Mod. Phys.* **93**, 015005 (2021).
- [7] C. Coullais, R. Fleury, J. van Wezel, Topology and broken Hermiticity, *Nat. Phys.* **17**, 9–13 (2021).
- [8] K. Ding, C. Fang, and G. Ma, Non-Hermitian topology and exceptional-point geometries, *Nat. Rev. Phys.* **4**, 745–760 (2022).
- [9] R. Lin, T. Tai, L. Li, and L. C. Lee, Topological non-Hermitian skin effect, *Front. Phys.* **18**, 53605 (2023).
- [10] L. Zhou and D.-J. Zhang, Non-Hermitian Floquet Topological Matter—A Review, *Entropy* **25**, 1401 (2023).
- [11] N. Okuma and M. Sato, Non-Hermitian Topological Phenomena: A Review, *Annu. Rev. Condens. Matter Phys.* **14**, 83–107 (2023).
- [12] A. Banerjee, R. Sarkar, S. Dey, and A. Narayan, Non-Hermitian topological phases: principles and prospects, *J. Phys.: Condens. Matter* **35**, 333001 (2023).
- [13] V. Meden, L. Grunwald, and D. M. Kennes, PT -symmetric, non-Hermitian quantum many-body physics—a methodological perspective, *Rep. Prog. Phys.* **86**, 124501 (2023).
- [14] C. M. Bender and D. W. Hook, PT -symmetric quantum mechanics, *Rev. Mod. Phys.* **96**, 045002 (2024).
- [15] K. Yang, Z. Li, J. L. K. König, L. Rødland, M. Stålhammar and E. J. Bergholtz, Homotopy, symmetry, and non-Hermitian band topology, *Rep. Prog. Phys.* **87**, 078002 (2024).
- [16] H. Wang, J. Zhong, and S. Fan, Non-Hermitian photonic band winding and skin effects: a tutorial, *Adv. Opt. Photon.* **16**, 659-748 (2024).
- [17] L.-M. Chen, Y. Zhou, S. A. Chen and P. Ye, Quantum Entanglement and Non-Hermiticity in Free-Fermion Systems, *Chinese Phys. Lett.* **41**, 127302 (2024).
- [18] M. V. Berry, Physics of nonhermitian degeneracies, *Czech. J. Phys.* **54**, 1039 (2004).
- [19] W. D. Heiss, The physics of exceptional points, *J. Phys. A: Math. Theor.* **45**, 444016 (2012).
- [20] B. Zhen, C. W. Hsu, Y. Igarashi, L. Lu, I. Kaminer, A. Pick, S.-L. Chua, J. D. Joannopoulos, and M. Soljačić, Spawning rings of exceptional points out of Dirac cones, *Nature (London)* **525**, 354 (2015).
- [21] K. Ding, G. Ma, M. Xiao, Z. Zhang, and C. T. Chan, Emergence, coalescence, and topological properties of multiple exceptional points and their experimental realization, *Phys. Rev. X* **6**, 021007 (2016).
- [22] B. Midya, H. Zhao, and L. Feng, Non-Hermitian photonics promises exceptional topology of light, *Nat. Commun.* **9**, 2674 (2018).
- [23] M.-A. Miri and A. Alu, Exceptional points in optics and photonics, *Science* **363**, eaar7709 (2019).
- [24] V. Martinez Alvarez, J. Barrios Vargas, and L. Foa Torres, Non-Hermitian robust edge states in one dimension: Anomalous localization and eigenspace condensation at exceptional points, *Phys. Rev. B* **97**, 121401(R) (2018).
- [25] S. Yao and Z. Wang, Edge States and Topological Invari-

- ants of Non-Hermitian Systems, *Phys. Rev. Lett.* **121**, 086803 (2018).
- [26] K. Yokomizo and S. Murakami, Non-Bloch band theory of non-Hermitian systems, *Phys. Rev. Lett.* **123**, 066404 (2019).
- [27] C. H. Lee and R. Thomale, Anatomy of skin modes and topology in non-Hermitian systems, *Phys. Rev. B* **99**, 201103(R) (2019).
- [28] N. Okuma, K. Kawabata, K. Shiozaki, and M. Sato, Topological origin of non-Hermitian skin effects, *Phys. Rev. Lett.* **124**, 086801 (2020).
- [29] Z. Yang, K. Zhang, C. Fang, and J. Hu, Non-Hermitian bulk-boundary correspondence and auxiliary generalized Brillouin zone theory, *Phys. Rev. Lett.* **125**, 226402 (2020).
- [30] J. Zhong, H. Wang, and S. Fan, Pole and zero edge state invariant for one-dimensional non-Hermitian sublattice symmetry, *Phys. Rev. B* **110**, 214113 (2024).
- [31] Z. Gong, Y. Ashida, K. Kawabata, K. Takasan, S. Higashikawa, and M. Ueda, Topological phases of non-Hermitian systems, *Phys. Rev. X* **8**, 031079 (2018).
- [32] K. Kawabata, K. Shiozaki, M. Ueda, and M. Sato, Symmetry and topology in non-Hermitian physics, *Phys. Rev. X* **9**, 041015 (2019).
- [33] C.-H. Liu, H. Jiang, and S. Chen, Topological classification of non-Hermitian systems with reflection symmetry, *Phys. Rev. B* **99**, 125103 (2019).
- [34] H. Zhou and J. Y. Lee, Periodic table for topological bands with non-Hermitian symmetries, *Phys. Rev. B* **99**, 235112 (2019).
- [35] C. C. Wojcik, X.-Q. Sun, T. Bzdušek, and S. Fan, Homotopy characterization of non-Hermitian Hamiltonians, *Phys. Rev. B* **101**, 205417 (2020).
- [36] M. Kotz and C. Timm, Topological classification of non-Hermitian Hamiltonians with frequency dependence, *Phys. Rev. Res.* **5**, 033043 (2023).
- [37] Q. Yan, B. Zhao, R. Zhou, R. Ma, Q. Lyu, S. Chu, X. Hu, and Q. Gong, Advances and applications on non-Hermitian topological photonics, *Nanophotonics* **12**, 2247-2271 (2023).
- [38] T. Yu, J. Zou, B. Zeng, J. W. Rao, and K. Xia, Non-Hermitian topological magnonics, *Phys. Rep.* **1062**, 1–86 (2024).
- [39] V. Montenegro, C. Mukhopadhyay, R. Yousefjani, S. Sarkar, U. Mishra, M. G. A. Paris, and A. Bayat, Review: Quantum metrology and sensing with many-body systems, *Phys. Rep.* **1134**, 1–62 (2025).
- [40] S. Kim, A. Krasnok, and A. Alù, Complex-frequency excitations in photonics and wave physics, *Science* **387**, eado4128 (2025).
- [41] S. Chen, A. Basit, L. Li, C. Hou, Y. Ruan, Y. Wei, and Z. Ni, Non-Hermitian Topological Lattice Photonics: An Analytic Perspective, *Adv. Photonics Res.* **2025**, 2500083 (2025).
- [42] C. Zhang, M. Kim, Y.-H. Zhang, Y.-P. Wang, D. Trivedi, A. Krasnok, J. Wang, D. Isleifson, R. Roshko, and C.-M. Hu, Gain-loss coupled systems, *APL Quantum* **2**, 011501 (2025).
- [43] Y.-W. Lu, W. Li, and X.-H. Wang, Quantum and Classical Exceptional Points at the Nanoscale: Properties and Applications, *ACS Nano* **19**, 17953–17978 (2025).
- [44] T. Scaffidi, D. E. Parker, and R. Vasseur, Gapless symmetry-protected topological order, *Phys. Rev. X* **7**, 041048 (2017).
- [45] J. Ruhman and E. Altman, Topological degeneracy and pairing in a one-dimensional gas of spinless fermions, *Phys. Rev. B* **96**, 085133 (2017).
- [46] R. Verresen, R. Moessner, and F. Pollmann, One-dimensional symmetry protected topological phases and their transitions, *Phys. Rev. B* **96**, 165124 (2017).
- [47] R. Verresen, N. G. Jones, and F. Pollmann, Topology and edge modes in quantum critical chains, *Phys. Rev. Lett.* **120**, 057001 (2018).
- [48] W. Berdanier, M. Kolodrubetz, S. A. Parameswaran, and R. Vasseur, Floquet quantum criticality, *Proc. Natl. Acad. Sci. USA* **115**, 9491 (2018).
- [49] D. E. Parker, T. Scaffidi, and R. Vasseur, Topological Luttinger liquids from decorated domain Walls, *Phys. Rev. B* **97**, 165114 (2018).
- [50] H.-C. Jiang, Z.-X. Li, A. Seidel, and D.-H. Lee, Symmetry protected topological Luttinger liquids and the phase transition between them, *Sci. Bull.* **63**, 753 (2018).
- [51] A. Keselman, E. Berg, and P. Azaria, From one-dimensional charge conserving superconductors to the gapless Haldane phase, *Phys. Rev. B* **98**, 214501 (2018).
- [52] D. Yates, Y. Lemonik, and A. Mitra, Central charge of periodically driven critical kitaev chains, *Phys. Rev. Lett.* **121**, 076802 (2018).
- [53] N. G. Jones and R. Verresen, Asymptotic correlations in gapped and critical topological phases of 1D quantum systems, *J. Stat. Phys.* **175**, 1164 (2019).
- [54] R. Verresen, Topology and edge states survive quantum criticality between topological insulators, arXiv:2003.05453.
- [55] C. M. Duque, H.-Y. Hu, Y.-Z. You, V. Khemani, R. Verresen, and R. Vasseur, Topological and symmetry-enriched random quantum critical points, *Phys. Rev. B* **103**, L100207 (2021).
- [56] R. Thorngren, A. Vishwanath, and R. Verresen, Intrinsically gapless topological phases, *Phys. Rev. B* **104**, 075132 (2021).
- [57] R. Verresen, R. Thorngren, N. G. Jones, and F. Pollmann, Gapless topological phases and symmetry-enriched quantum criticality, *Phys. Rev. X* **11**, 041059 (2021).
- [58] R. R. Kumar, Y. R. Kartik, S. Rahul, and S. Sarkar, Multicritical topological transition at quantum criticality, *Sci. Rep.* **11**, 1004 (2021).
- [59] U. Borla, R. Verresen, J. Shah, and S. Moroz, Gauging the Kitaev chain, *SciPost Phys.* **10**, 148 (2021).
- [60] M. Jangjan and M. V. Hosseini, Topological phase transition between a normal insulator and a topological metal state in a quasi-one-dimensional system, *Sci. Rep.* **11**, 12966 (2021).
- [61] X.-J. Yu, R.-Z. Huang, H.-H. Song, L. Xu, C. Ding, and L. Zhang, Conformal boundary conditions of symmetry-enriched quantum critical spin chains, *Phys. Rev. Lett.* **129**, 210601 (2022).
- [62] A. Cerjan and T. A. Loring, Local invariants identify topology in metals and gapless systems, *Phys. Rev. B* **106**, 064109 (2022).
- [63] A. J. Friedman, B. Ware, R. Vasseur, and A. C. Potter, Topological edge modes without symmetry in quasiperiodically driven spin chains, *Phys. Rev. B* **105**, 115117 (2022).
- [64] N. G. Jones, R. Thorngren, and R. Verresen, Bulk-boundary correspondence and singularity-filling in long-range free-fermion chains, *Phys. Rev. Lett.* **130**, 246601 (2023).

- (2023).
- [65] R. Wen and A. C. Potter, Bulk-boundary correspondence for intrinsically gapless symmetry-protected topological phases from group cohomology, *Phys. Rev. B* **107**, 245127 (2023).
- [66] R. R. Kumar, N. Roy, Y. R. Kartik, S. Rahul, and S. Sarkar, Signatures of topological phase transition on a quantum critical line, *Phys. Rev. B* **107**, 205114 (2023).
- [67] R. R. Kumar, Y. R. Kartik, and S. Sarkar, Topological phase transition between non-high symmetry critical phases and curvature function renormalization group, *New J. Phys.* **25**, 083027 (2023).
- [68] S. Prembabu, R. Thorngren, and R. Verresen, Boundary-deconfined quantum criticality at transitions between symmetry-protected topological chains, *Phys. Rev. B* **109**, L201112 (2024).
- [69] L. Li, M. Oshikawa, and Y. Zheng, Decorated defect construction of gapless-SPT states, *SciPost Phys.* **17**, 013 (2024).
- [70] X.-J. Yu, S. Yang, H.-Q. Lin, and S.-K. Jian, Universal entanglement spectrum in one-dimensional gapless symmetry protected topological states, *Phys. Rev. Lett.* **133**, 026601 (2024).
- [71] X.-J. Yu and W.-L. Li, Fidelity susceptibility at the Lifshitz transition between the noninteracting topologically distinct quantum critical points, *Phys. Rev. B* **110**, 045119 (2024).
- [72] W.-H. Zhong, W.-L. Li, Y.-C. Chen, and X.-J. Yu, Topological edge modes and phase transitions in a critical fermionic chain with long-range interactions, *Phys. Rev. A* **110**, 022212 (2024).
- [73] H.-L. Zhang, H.-Z. Li, S. Yang, and X.-J. Yu, Quantum phase transition and critical behavior between the gapless topological phases, *Phys. Rev. A* **109**, 062226 (2024).
- [74] L. Su and M. Zeng, Gapless symmetry-protected topological phases and generalized deconfined critical points from gauging a finite subgroup, *Phys. Rev. B* **109**, 245108 (2024).
- [75] X. Wen, Exactly solvable non-unitary time evolution in quantum critical systems I: effect of complex spacetime metrics, *J. Stat. Mech.* **2024**, 103103 (2024).
- [76] L. Zhou, J. Gong, and X.-J. Yu, Topological edge states at Floquet quantum criticality, *Commun. Phys.* **8**, 214 (2025).
- [77] L. Zhou, R. Wang, and J. Pan, Gapless higher-order topology and corner states in Floquet systems, *Phys. Rev. Res.* **7**, 023079 (2025).
- [78] G. Cardoso, H.-C. Yeh, L. Korneev, A. G. Abanov, and A. Mitra, Gapless Floquet topology, *Phys. Rev. B* **111**, 125162 (2025).
- [79] S.-J. Huang, Fermionic quantum criticality through the lens of topological holography, *Phys. Rev. B* **111**, 155130 (2025).
- [80] J. Fang, Q. Zhou, and X. Wen, Phase transitions in quasiperiodically driven quantum critical systems: analytical results, *Phys. Rev. B* **111**, 094304 (2025).
- [81] L. Li, M. Oshikawa, and Y. Zheng, Intrinsically/purely gapless-SPT from non-invertible duality transformations, *SciPost Phys.* **18**, 153 (2025).
- [82] S.-J. Huang and M. Cheng, Topological holography, quantum criticality, and boundary states, *SciPost Phys.* **18**, 213 (2025).
- [83] R. Wen and A. C. Potter, Classification of 1+1D gapless symmetry protected phases via topological holography, *Phys. Rev. B* **111**, 115161 (2025).
- [84] L. Zhou, F. Zhang, and J. Pan, Floquet Möbius topological insulators, arXiv:2506.01401.
- [85] L. D. Landau and E. M. Lifshitz, *Statistical Physics, Part 1, 3rd Edition* (Course of Theoretical Physics, Vol. 5) (Elsevier, 2013).
- [86] S. Ryu, A. P. Schnyder, A. Furusaki and A. W. W. Ludwig, Topological insulators and superconductors: tenfold way and dimensional hierarchy, *New J. Phys.* **12**, 065010 (2010).
- [87] Z. Zhang, U. Agrawal, and S. Vijay, Quantum communication and mixed-state order in decohered symmetry-protected topological states, *Phys. Rev. B* **111**, 115141 (2025).
- [88] X.-D. Dai, Z. Wang, H.-R. Wang, and Z. Wang, Steady-state topological order, *Phys. Rev. B* **111**, 115142 (2025).
- [89] L. A. Lessa, M. Cheng, and C. Wang, Mixed-State Quantum Anomaly and Multipartite Entanglement, *Phys. Rev. X* **15**, 011069 (2025).
- [90] T.-T. Wang, M. Song, Z. Y. Meng, and T. Grover, Analog of Topological Entanglement Entropy for Mixed States, *PRX Quantum* **6**, 010358 (2025).
- [91] Y. Guo, J.-H. Zhang, H.-R. Zhang, S. Yang, and Z. Bi, Locally Purified Density Operators for Symmetry-Protected Topological Phases in Mixed States, *Phys. Rev. X* **15**, 021060 (2025).
- [92] S. Sun, J.-H. Zhang, Z. Bi, and Y. You, Holographic View of Mixed-State Symmetry-Protected Topological Phases in Open Quantum Systems, *PRX Quantum* **6**, 020333 (2025).
- [93] J. K. Asbóth, L. Oroszlány, and A. Pályi, *A Short Course on Topological Insulators* (Springer Cham, New York, 2016).